

## Chapter 7

# Interferometric Synthetic Aperture Radar (IfSAR)

Scott Hensley and Lorraine Tighe

## TECHNOLOGY OVERVIEW

Remotely sensed methods are the most efficient methods for generating digital elevation models, especially over large geographic areas. While the success of traditional optical sensors has been well documented, in regions of persistent cloud cover, they are not able to obtain full coverage data. Radar sensors on the other hand, can penetrate clouds and operate at night.

Combining conventional synthetic aperture radar (SAR) and interferometry creates what is commonly known as IfSAR (also written as InSAR), providing a 24/7 all-weather three-dimensional mapping technique that has been commercially available since the mid-1990's. Since then, the IfSAR technique has been used to map the entire landmass of the Earth (from pole-to-pole) providing a homogeneous high resolution digital elevation model with an unrivalled accuracy and quality that surpasses that of any global optical-based DEM available today.

The main objectives of this chapter are to provide DEM users with an overview of the IfSAR topographic mapping technique and the operating principles as they relate to commercially available systems to include the STAR systems operated by Intermap Technologies Inc., the GeoSAR system operated by Fugro EarthData Inc., and various satellite SAR systems. The advantages and disadvantages of such systems are reviewed. Practical information regarding the collection, processing, products, and quality assessment of IfSAR DEM data are discussed. The chapter closes with examples of applications for use with IfSAR derived DEMs, to include Dewberry' ongoing aerial IfSAR mapping of Alaska with data acquired by Intermap and Fugro.

This chapter has been modified considerably from the first and second editions of the DEM Users Manuals. Readers interested in more of the physics and history of IfSAR techniques, hardware, system engineering or signal processing are recommended to consult [Richards, 2007, Rosen 2000] and the previous editions of the DEM User's Manual.

## **SAR Explained**

RADAR, which stands for "radio detection and ranging," subsequently referred to as radar, is an active remote sensing instrument that operates in the microwave portion of the electromagnetic spectrum. It provides its own source of illumination in the form of microwave pulses that are transmitted to the terrain being imaged. Therefore, radar sensors operate independently of the sun, often collecting data during night.

To obtain high resolution data from radar sensors, a synthetic aperture radar (SAR) configuration is implemented. SAR is a form of radar where the radar antennae, onboard a platform (air or space), transmit radio waves in the form of a wide beam of high-power pulses ('echoes') of microwave energy to the area being imaged (Elachi 1988). Radar

pulses are transmitted toward the terrain of interest in a vertically oblique direction that intersects the terrain with an oval footprint elongated in the range direction (e.g. across track; Figure 7.1). Consequently, two different scanning mechanisms are employed: one in the range direction, the second in the azimuth direction (direction of flight). In the range direction each transmitted pulse sweeps across the swath at the velocity of light. In the azimuth direction, the swath is scanned in the along-track direction at the speed of the antenna footprint (or forward movement of the platform). These two mechanisms differ in timescales from each other by several orders of magnitude, which allows us to treat them as mutually independent (Bamler and Hartl, 1998).

SAR sensors record the interference (Doppler) pattern from echo signals over several hundred to several thousand meters along the flight path. The received echoes form the raw data matrix or complex image containing amplitude and phase. The coordinates of the 2D raw signal image are range for the distance of the scatterer from the SAR (or equivalently echo delay time) and azimuth for the position of the scatterer along the sensor path (Figure 7.1). The target of interest is imaged (illuminated) several hundred times from different locations along the flight path generating numerous echoes that are recorded coherently (i.e., amplitude and phase as a function of time).

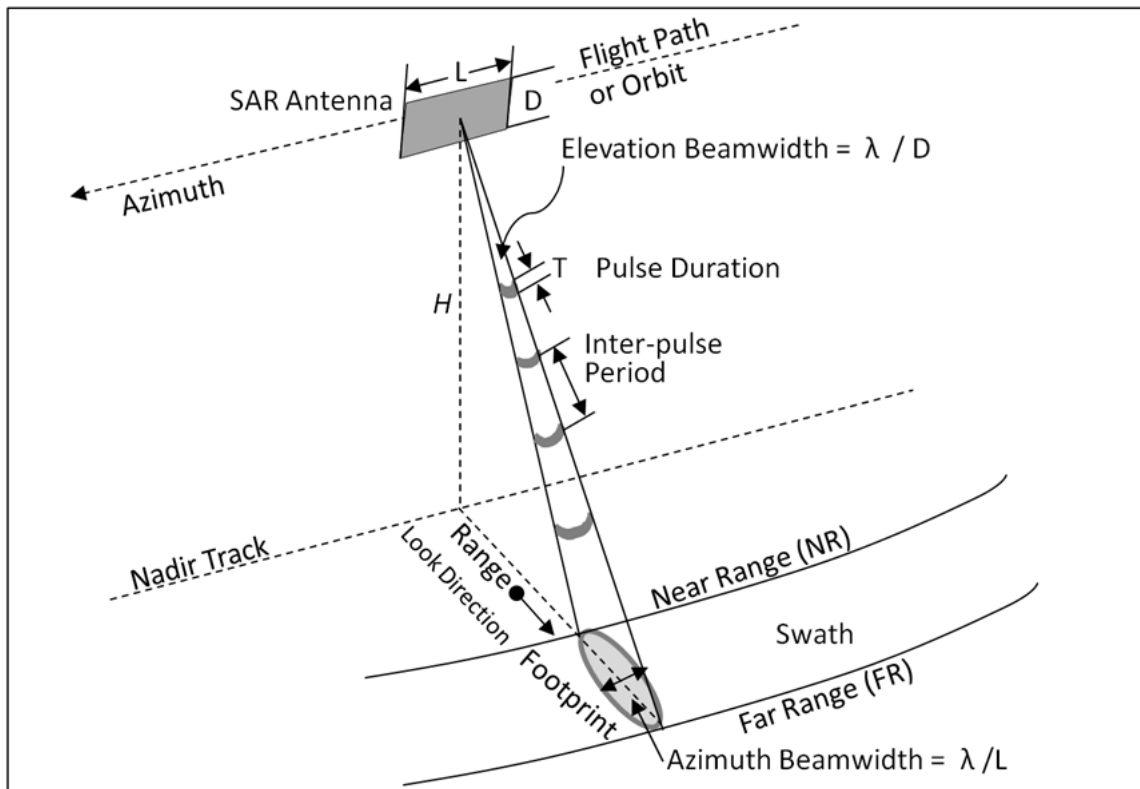


**Figure 7.1.** Scanning configuration for a right-hand looking rectangular SAR antenna, modified after Olmsted (1993).  $L$  is the antenna length,  $D$  is the antenna width,  $T$  is the pulse duration, and  $H$  is the Nadir Range. The recorded signal data (amplitude and phase) can produce a two-dimensional radar image. The distance measured between the antenna and the target is known as slant range.

The accepted parameter for discussion of a radar system's "resolution" performance is impulse response. The microwave pulses are combined to synthesize a linear array with angular resolution equivalent to an antenna several hundred meters in length, resulting in

what is called the azimuth resolution, in the direction parallel to the sensor flight path and the range resolution, perpendicular to the flight path direction. Azimuth impulse response is a function of antenna beam-width and the number of azimuth looks processed, whereas range resolution is a function of the range bandwidth. Azimuth resolution is equal to approximately one-half the actual (real) antenna length ( $L/2$ ) and does not depend on platform altitude (distance). Range resolution, on the other hand, is determined by the transmitted pulse width ( $T$  in Figure 7.1; e.g. narrow pulses yield fine range resolution (Elachi, 1988)). Range is determined by precisely measuring the time from transmission of a pulse to receiving the echo from a target.

Microwaves are transversal waves, for example, in the direction of propagation the electric and magnetic fields are mutually orthogonal. By convention, polarized electromagnetic radiation is described by specifying the orientation of the wave's electric field at a point in space over one period of oscillation. Most earth observation SARs systems use Linear (or planar) polarizations where the vibration of the electric field vector is in a parallel direction to the propagating wave. The radar signals can be set up to vibrate in either a horizontal (H) or vertical (V) plane or in a circular fashion. Antennae can transmit in one plane and receive in another. Possible variations are HH, VV, HV, and VH for: horizontal transmit, horizontal receive; vertical transmit, vertical receive; and so on. All four polarizations are typically denoted as "Quad" polarization.

Targets on the Earth's surface scatter microwave radiation differently depending on the polarization of the wave transmitted. Volume scattering (illustrated in Figure 7.10) is the main interaction in vegetated canopies. It causes the incoming signal to be depolarized, for example, the signal is scattered in other directions, at different relative vibrational planes. A H-polarized wave might hit a tree, bounce back and forth among leaves/twigs, and be backscattered to the SAR sensor in a V-polarized state. Using an HV setup, the antenna could receive these V-polarized returns. Though the overall radar backscatter received would be less than, say, a VV setup, the resulting image would have increased variation between regions of volume scattering (higher potential to return V-polarized backscatter - usually vegetation) and regions of surface scattering.

SAR systems are not impeded by darkness, atmospheric conditions such as haze, clouds, light rain, or smoke (Bamler and Hartl, 1998). The resulting microwave energy can produce two-dimensional cloud free radar images. These have significant advantages over optical systems providing a suitable sensor technology for nearly all weather and day or night data acquisitions, across the globe. SAR systems require a complex integrated array of onboard navigational and control systems with location accuracy provided by both Doppler and

inertial navigation equipment. The outputs produced are typically two-dimensional (2D) SAR imagery.

### Basic Concept and Operating Principles

As with many topographic mapping techniques the location of a point on the ground is determined in three dimensions by solving for an unknown component of a triangle associated to the observation geometry. In the case of IfSAR, the triangle is created by the physical separation (in space or in time) of two SAR apertures' (SAR Antenna  $A_1$  and SAR Antenna  $A_2$ ) in the across-track plane (perpendicular to the flight direction) and the distance from the apertures to the point on the ground (P) being measured (illustrated by the red triangle in Figure 7.2). Radar pulses are transmitted from one or both SAR antenna(s), radar echoes are received by both the SAR antennas. If the received signals from the two antennas are combined *coherently* for each imaged point to measure the phase difference, then the system forms an **interferometric SAR**. More detail on IfSAR systems and processing can be found in [Rosen et al, 2000], [Madsen and Zebker, 1999], and [Bamler and Hartl, 1998].

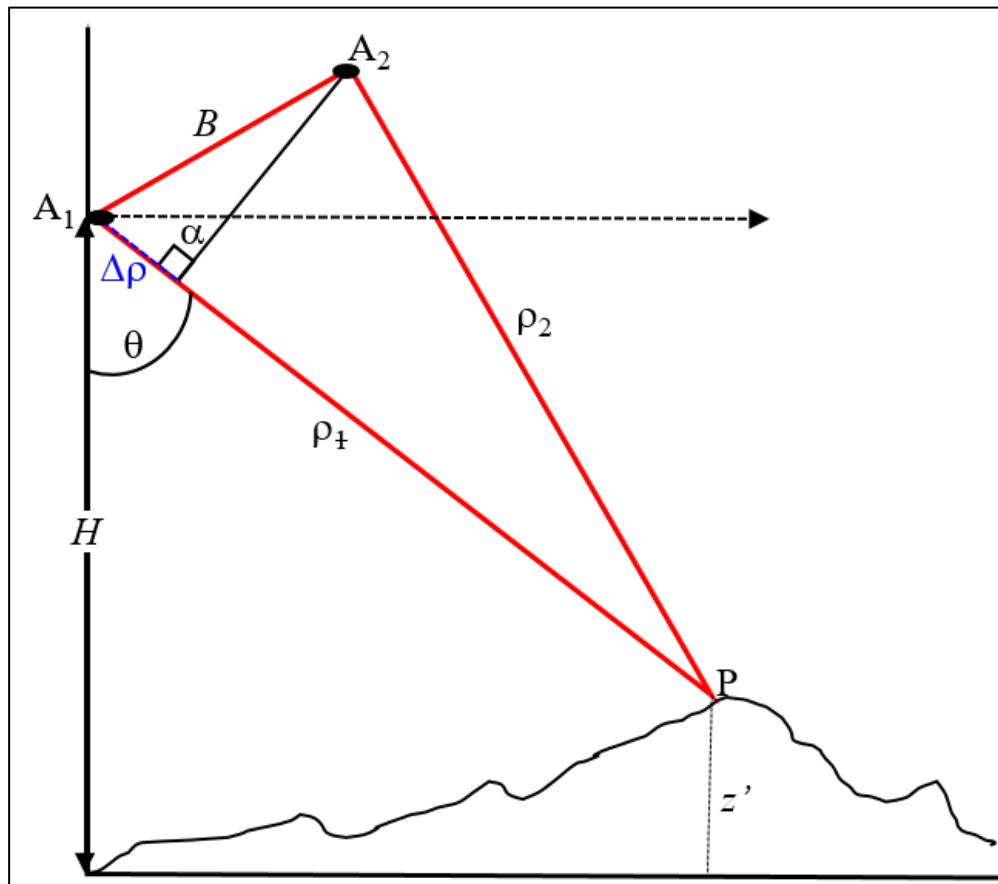


Figure 7.2. Simplified broadside looking (zero Doppler) radar interferometry geometry. The difference in range from the two observing antennas ( $A_1$ ,  $A_2$ ) to the target (P) is approximately equal to the projection of the baseline vector onto the line-of-sight vector shown in blue ( $\Delta\rho$ ). This range difference can be related to a phase measurement using equation 7.1 and forms the primary **interferometric** observable used to derive topographic height measurements. Parameters in this figure are defined following discussion of Equation 7.1.

The interferometric phase difference is essentially related to the geometric path length ( $\Delta\rho$ ) difference to the image point, which depends on the topography. With knowledge of the interferometer geometry, the phase difference can be converted into an altitude for each image point. By having a third measurement, the **interferometric** phase, in addition to the standard cross-track location of an image point obtained with the SARs ( $A_1$  and  $A_2$ ), it is possible to determine the three-dimensional location of a point (P) shown in Figure 7.2.

By measuring the time, it takes a radar pulse to propagate from the SAR antenna to a target and return, the distance or range measurements are related to phase measurements by converting the distance to units of wavelength and recalling each wavelength corresponds to  $2\pi$  radians or  $360^\circ$  of phase (Figure 7.3). Phase measurements in interferometric systems can be made with degree level accuracy, and with typical wavelengths in the range of 2-20 cm, corresponds to measurements having millimeters to centimeter accuracy.

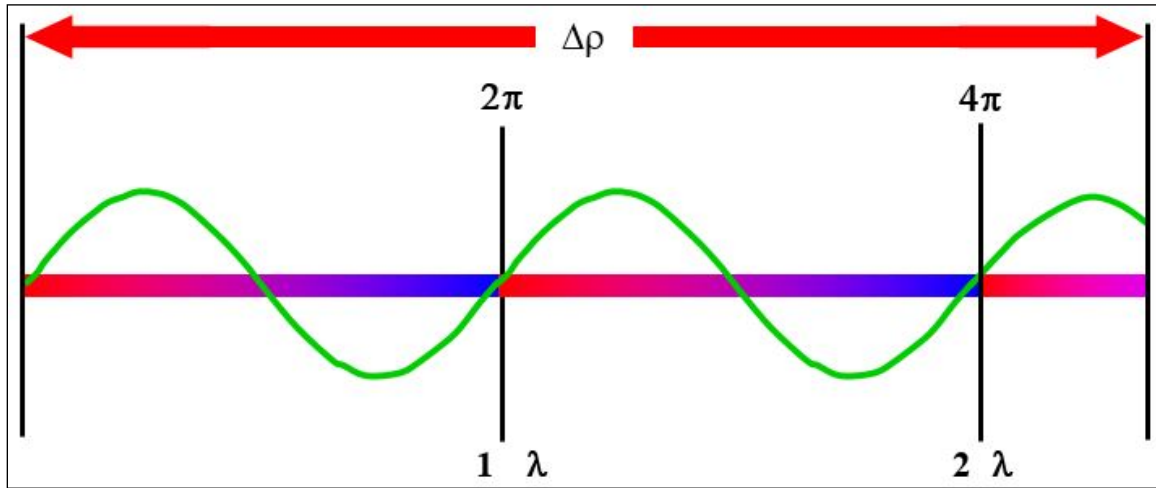


Figure 7.3. Illustration of the relationship between phase, distance, and **wavelength**.

The path length difference,  $\Delta\rho$ , of the signals received by the two antennas is approximately given by

$$\Delta\rho = |\vec{\rho}_2| - |\vec{\rho}_1| \approx B\sin(\theta-\alpha) \quad (7.1)$$

where  $\vec{\rho}_1$  indicates the vector from antenna 1 to the target (P), B is the length of the baseline vector which is the vector pointing from antenna 1 to antenna 2,  $\theta$  is the desired elevation (or look) angle and the baseline orientation angle,  $\alpha$ , is the angle the baseline vector makes with respect to the horizontal. Observe that the range difference to a good approximation for most systems is simply the length of the projection of the baseline vector onto the line-of-sight. The range difference,  $\Delta\rho$ , may be obtained by measuring  $\phi$ , the phase between the two interferometer signals, using the relation

$$\phi = -\frac{2\pi m \Delta\rho}{\lambda} \quad m = 1, 2 \quad (7.2)$$

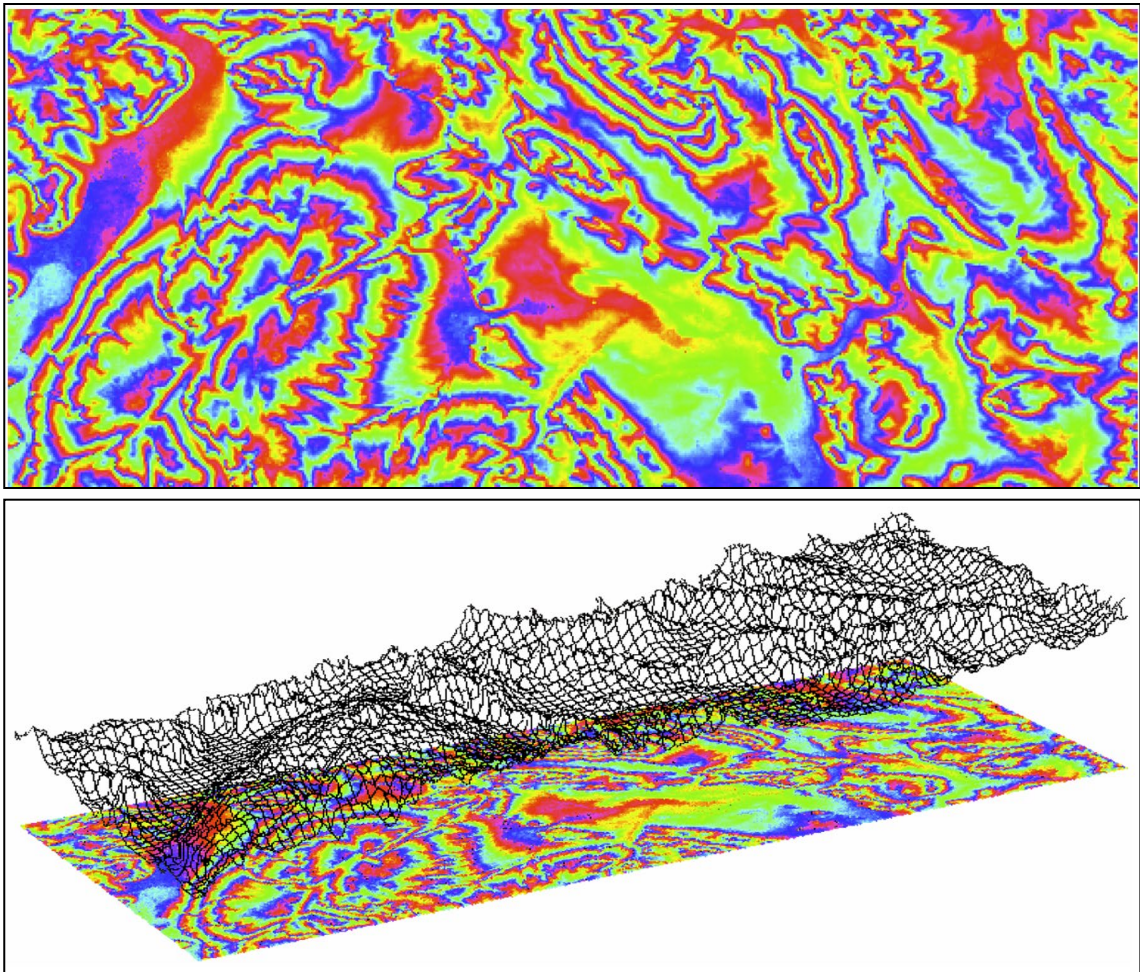
where  $\lambda$  is the radar wavelength and  $m$  equals 1 when using a single transmit antenna, or 2 when transmitting from two antennas, the so-called Ping-Pong mode, or for repeat pass systems described below. Using the simplified geometry of Figure 7.2 the height of a target,  $z'$ , is given by

$$z' = H - \rho \cos(\theta) \tag{7.3}$$

where  $H$  is the altitude of the radar antenna and  $\rho$  is the slant range from the antenna to the target. Since the signal phase is sensitive to displacements between images of a fraction of a wavelength, the interferometric technique provides a very accurate means of determining topographic heights. Using Equations 7.1 and 7.2 the elevation angle can be determined to be

$$\theta = \sin^{-1} \left( \frac{\lambda \phi}{2\pi m B} \right) + \alpha \tag{7.4}$$

It is immediate from Equations 7.3 and 7.4 that determining the height of a target requires knowledge of the platform position, the range, the interferometric baseline length, the baseline angle and the interferometric phase. Generation of accurate topographic maps using radar interferometry places stringent requirements on the knowledge of the platform



and baseline vectors. Figure 7.4 provides an example of interferometric phase measurements (interferogram) and elevation data.

Figure 7.4. Interferometric phase and associated elevation data generated from single pass IfSAR observations. Top image: IfSAR interferogram where one set of colors (pink, red, yellow, green, and blue) represents one  $0 - 2\pi$  interferometric fringe. Middle Image: the interferogram (bottom) has been processed to unwrap the phase data to derive a DSM represented by the wire mesh and Lower image) generated from single pass IfSAR observations [modified after Gens, 2002].

Understanding conditions when interferometric phase measurements useful for topographic mapping are possible requires us to examine more closely what happens to radar signals within a resolution element. Consider a resolution cell with elemental scatterers arranged throughout as shown in Figure 7.5. Each elemental scatterer will contribute a portion of the backscatter that is added coherently with the other elemental scatterers to produce the return from the cell. Since the return from the elemental scatterers adds coherently, the relative phase or distance between the scatterers affects the magnitude and phase of the total signal. Conceptually, the phase can be decomposed into a systematic and random component by selecting the center of the cell as reference. The systematic component is the phase from the antenna to the center of the cell and is the portion of the signal needed for interferometry. The random component is the coherent sum of the signals from the randomly arranged elemental scatterers within the cell to the center of the cell. This component, although random from resolution element to resolution element, remains the same (or nearly the same) if the viewing geometry is nearly identical and if the relative position of the elemental scatterers within a cell remain the same (or nearly the same) as shown in Figure 7.5.

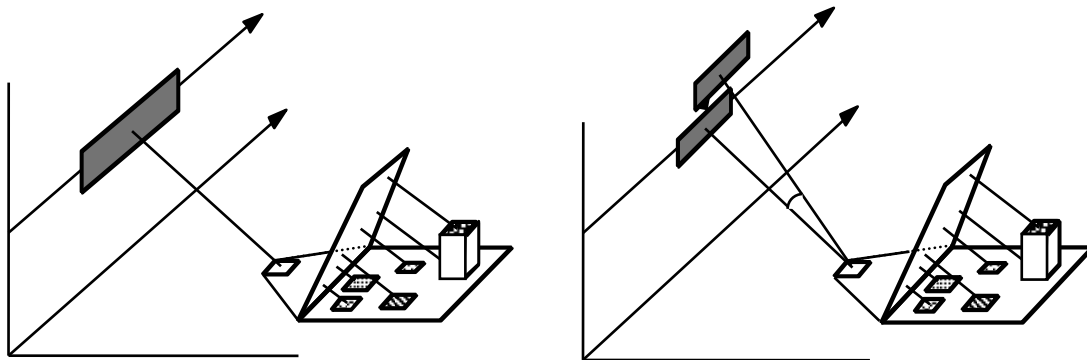


Figure 7.5. The left portion of the figure shows a notional arrangement of elemental scatterers within an imaging cell. Each elemental scatterer may have different surface roughness and dielectric properties as indicated by the different shading patterns. The right portion of the figure shows that if the imaging geometry is nearly the same the relative distance between scatterers is preserved and cancels out in the interferometric phase measurement.

For interferometric applications, where the viewing geometry of the interferometric pair is nearly the same, the random component arising from the elemental scatterer arrangement cancels and leaves only the difference between systematic components. This phase difference is the interferometric phase measurement and equals the phase in Equation 7.2 modulo  $2\pi$ . Another random component, which does not cancel, is thermal noise. Thermal noise is different for each receiving antenna, and depending on its magnitude relative to the desired signal degrades interferometric phase measurement. The above discussion is summarized below.

$$\text{phase} = \underbrace{\text{range from antenna to center of cell}}_{\text{Systematic component desired by interferometric measurement}} + \underbrace{\text{Coherent sum of elemental scatterers arranged randomly in cell}}_{\text{Random component that if look direction is nearly the same and scatterers within cell do not move relative to each other this component cancels in the interferogram formation process.}} + \underbrace{\text{thermal noise}}_{\text{Random component that does not cancel and results in interferometric phase noise}}$$

It is important to appreciate the consequences of the fact the interferometric phase measurement is made modulo  $2\pi$ . The total range difference between the two observations that the phase represents in general can be many multiples of the radar wavelength, or expressed in terms of phase, many multiples of  $2\pi$ . It is this value that is required to make height measurements. The standard approach for determining the unique phase that is directly proportional to the range difference is to first determine the relative phase between pixels via the so-called “**phase unwrapping**” process. Unwrapping of IfSAR imagery is a non-trivial process for which several algorithms have been developed. Complications arise in avoiding unwrapping errors in regions of shadow, layover and low signal return. The connected phase field after unwrapping may still need to be adjusted by an overall constant of  $2\pi$ . The step that determines the overall constant of  $2\pi$  is referred to as **absolute phase determination**.

**Interferometric correlation**, a measure of the similarity of the signal received at the two antennas, can be estimated directly from the image data of the two interferometric channels [Zebker and Villasenor, 1992]. Correlation measurements have values between 0 and 1, with 1 designating perfect correlation between the channels. Sometimes it is more convenient to refer to the amount of **interferometric decorrelation**, which is defined as one minus the correlation. The amount of decorrelation due to the slightly different viewing geometry is called **geometric decorrelation**. Thermal noise induced signal decorrelation is called **noise decorrelation**. Shadowed regions suffer from noise decorrelation and areas on steep slopes exhibit geometric decorrelation that increases phase noise and can preclude useful phase measurements altogether. Another form of decorrelation occurs when there is a vertical distribution of scattering elements within a resolution element as shown in Figure 7.6. Not only is the signal decorrelated, the point within the resolution cell corresponding to the interferometric phase measurement depends on the wavelength and the scatterer distribution in the cell. This form of decorrelation is called **volumetric decorrelation** and can be used to infer information about the vertical structure of the volume. Recently, there has been a great deal of activity using volumetric correlation to estimate tree and canopy structure within the interferometric SAR community.



Figure 7.6. Vertical structure of scatterers within a resolution element due to vegetation or other structures present in the cell cause increased decorrelation. This form of **decorrelation** can be used to infer information about vertical structure within a resolution element. The increased decorrelation results from the increased size of the range cell projected back toward the direction of the radar (shown in magenta) when compared to a flat surface.

There is an upper value on the useful baseline length known as the critical baseline [Rosen et al, 2000]. The critical baseline is reached when the amount of phase change per resolution element exceeds  $2\pi$  radians. This limitation is a result of the fact that the interferometric phase measurement is made only modulo  $2\pi$ . As the baseline approaches the critical **baseline**, the phase values from the two antennas become completely decorrelated. However, as the baseline increases, the sensitivity of phase to height increases improving the accuracy of interferometric SAR systems. Practical mapping systems must select baselines with a balance between adequate phase to height sensitivity to meet mapping requirements and excessive decorrelation with corresponding processing difficulties.

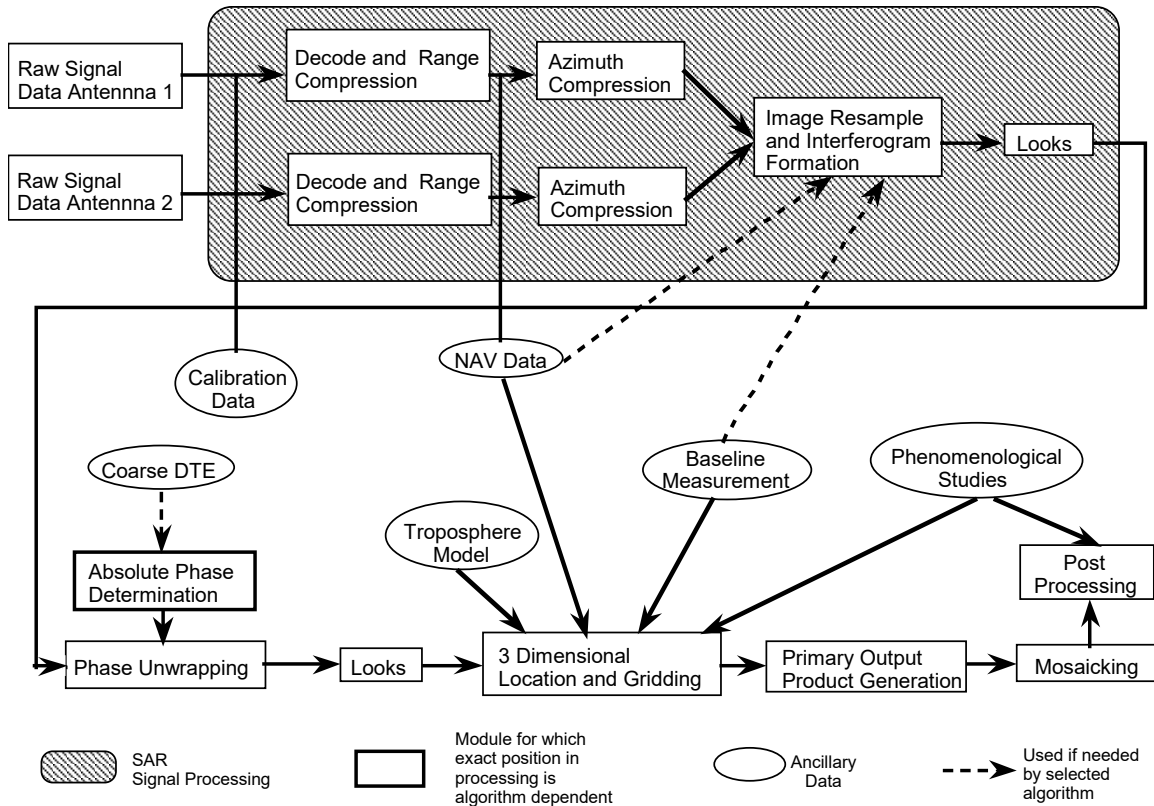


Figure 7.7. **Interferometric processing** block diagram.

After the multi-looked **interferogram** has been generated the phase for each complex sample is computed. To generate a continuous height map, the two-dimensional phase field must be unwrapped. After the unwrapping process an overall multiple of  $2\pi$  is estimated and added to the unwrapped phase (the estimated value may be 0).

Combining the SAR image formation process, interferometric phase measurement, unwrapping and height determination into an automated processing algorithm has a process flow that is shown in Figure 7.7 [Madsen et al, 1993]. An understanding of the steps involved is useful for understanding IfSAR calibration and for identifying potential error sources in IfSAR generated DEMs. Raw data are collected and stored onboard for batch processing. The first processing step is decoding the byte data, followed by range compression for each of the two interferometric channels. Using the platform motion information obtained from **Inertial Navigation System (INS)** and **Global Positioning System (GPS)** measurements, as well as any other baseline metrology devices, the data are

compensated for perturbations in aircraft motion from a reference path<sup>1</sup> and then azimuth compressed. This generates two single-look complex images.

One image of the single-look complex image pair is resampled to overlay the other. This registration must be done to a small fraction of a pixel (typically less than .1 of a pixel) to avoid phase **decorrelation**. Multiplying the complex pixel value in one image by the complex conjugate of the corresponding pixel value in the second image forms an **interferogram**. The resulting interferogram is multi-looked, by spatially averaging the complex pixels in a box about a given pixel to reduce the amount of phase noise.

After determining the absolute phase for each pixel in the interferogram and possibly taking additional looks, the 3-dimensional target position can be determined. Phase corrections are applied to the interferometric phase to account for tropospheric effects, and the range is corrected to account for the speed of light changes in the atmosphere. Using accurate baseline and platform position information, the phase and range information for the target position is computed. A relief map is generated by gridding the unevenly sampled 3-dimensional target locations in a natural coordinate system aligned with the flight path. The gridded products include the target heights, the SAR image which has been orthorectified, a **correlation map**, and a **height error map** described below. These four products will be referred to as primary mapping or strip map products. The resulting radar relief map may be measuring the heights above the ground, within the vegetation canopy or beneath the surface, in arid regions. To convert this map into a true ground surface DEM, corrections based on phenomenological studies, e.g. using scattering or semi-empirical curves to correct elevation measurements based on the amount of decorrelation in the canopy, must be incorporated into either the 3-dimensional location algorithms or into a post processing step.

One of the unique aspects of **interferometric SAR** systems is the ability to determine the statistical height precision, that is the degree of height noise from pixel to pixel, estimated from knowledge of the correlation,  $\gamma$  [Hensley and Webb, 1994]. The amount of phase noise between the two channels is simply and directly related to the correlation and number of looks used to reduce phase noise<sup>2</sup>. The **Cramer-Rao bound** relating the phase variance,  $\sigma_{\phi}$ , to the correlation coefficient,  $\gamma$ , is given by

$$\sigma_{\phi} = \frac{1}{\sqrt{2N_L}} \frac{\sqrt{1-\gamma^2}}{\gamma} \quad (7.5)$$

where  $N_L$  is the number of looks. From Equations 7.3 and 7.4 the height error,  $\sigma_h$ , as a function of the phase noise is found to be

---

<sup>1</sup> The process of correction for motion away from an ideal path is referred to as **motion compensation**. Motion compensation corrects for motion on the order of fractions of a wavelength to generate well focused SAR imagery. The requirements for motion compensation are even more demanding for IfSAR systems and place stringent requirements on the platform and baseline metrology systems.

<sup>2</sup> The **Cramer-Rao bound** used to relate the phase noise to correlation and number of looks is only valid when the number of looks exceeds 4 or 5. The number of looks in most interferometric systems used to generate topographic maps usually is much larger than 4. A notable exception is the **SRTM** system (described later in the chapter) where the number of looks varied between 1 and 4.

$$\sigma_h = \frac{\lambda \rho \sin(\theta)}{2\pi m B \cos(\theta - \alpha)} \sigma_\phi \quad (7.6)$$

Equations 7.5 and 7.6 allow the generation of an error map showing the local height accuracy for each post in an interferometrically derived DEM.

Typically, the post spacing of the IfSAR topographic data are comparable to the fine spatial resolution of SAR imagery while the altitude measurement accuracy generally exceeds stereoscopic accuracy at comparable resolutions. The registration of the two SAR images for the interferometric measurement, the retrieval of the **interferometric phase difference** and subsequent conversion of the results into digital elevation models of the terrain can be highly automated, representing an intrinsic advantage of the IfSAR approach. The performance of IfSAR systems is largely understood both theoretically and experimentally enabling these systems to be designed and built to meet specific mapping objectives. These developments have led to airborne and spaceborne IfSAR systems for routine topographic mapping.

For the remainder of this chapter IfSAR is defined as an airborne or spaceborne interferometric radar system, flown aboard rotary or fixed wing aircraft, or any space based platform, that is used to acquire 3-dimensional coordinates (these coordinates must be convertible to a specified geographic datum) of terrain and terrain features that are both manmade and naturally occurring. IfSAR systems consist of a platform, GPS and attendant GPS base station(s) if needed, INU and interferometric radar system including commanding and data acquisition systems. The system may also include other ancillary equipment such as baseline metrology systems as necessary for accurate map generation. These systems form synthetic aperture images of terrain surfaces from two spatially separated antennas over an imaged swath that may be located to the left, right or both sides of the imaging platform.

### **SAR Wavelength**

Most geoscientists refer to SAR systems in terms of their wavelength,  $\lambda$ , denoted by a letter code (assigned in World War II for security reasons). The most common wavelengths for SAR remote sensors are labeled K, X, C, L, S, and P, listed in order of increasing wavelength size (Table 7.1). To appreciate why particular radar frequencies (wavelengths) are selected for a given application, it is necessary to have a cursory understanding of how radar signals interact with terrain [Elachi, 1988], [Raney, 1999]. Each pixel in a SAR image is a complex number having a magnitude and phase determined by the terrain surface properties and the image geometry. A radar signal impinging on a resolution element (area of the surface contained within a single range and azimuth bin) will in general scatter energy in all directions. The signal reflected toward the radar is referred to as the backscatter. **Backscatter** strength is a function of the composition of the surface and its structure. Wavelength selection is often a trade among scientific considerations, technology readiness, platform constraints, availability and cost.

**Table 7.1. SAR Band, Wavelength and Frequency Relationship**

<b>SAR Band Identification</b>	<b>Wavelength Range (cm)</b>	<b>Frequency Band (MHz)</b>
Ka	1.13-.75	26500-40000

K	1.66-1.13	18000-26500
Ku	2.4-1.66	12500-18000
X	3.75-2.4	8000-12500
C	7.5-3.75	4000-8000
S	15-7.5	2000-4000
L	30-15	1000-2000
P or UHF	100-30	300-900
VHF	1000-100	30-300
HF	10000-1000	3-30

Elevations derived from IfSAR methods are determined from the scattering phase centre height (denoted as  $h_{\text{spc}}$ ). The  $h_{\text{spc}}$  is a type of amplitude weighted average of all vertically distributed scattering elements within a resolution cell. The SAR wavelength, baseline and vertical structure of the scattering medium determines the  $h_{\text{spc}}$ . The location of  $h_{\text{spc}}$  depends on the penetration depth of microwaves into the canopy (Figure 7.8), which depends primarily on the SAR wavelength in addition to other parameters such as the size and density distribution of the scattering elements, the geometric arrangement of the scatterers, canopy moisture condition, surface roughness, and moisture content of the ground layer. For example, at X-band wavelength the  $h_{\text{spc}}$  is at or very near bare ground in barren areas whereas, in forest it is closer to the canopy top (Figure 7.8)

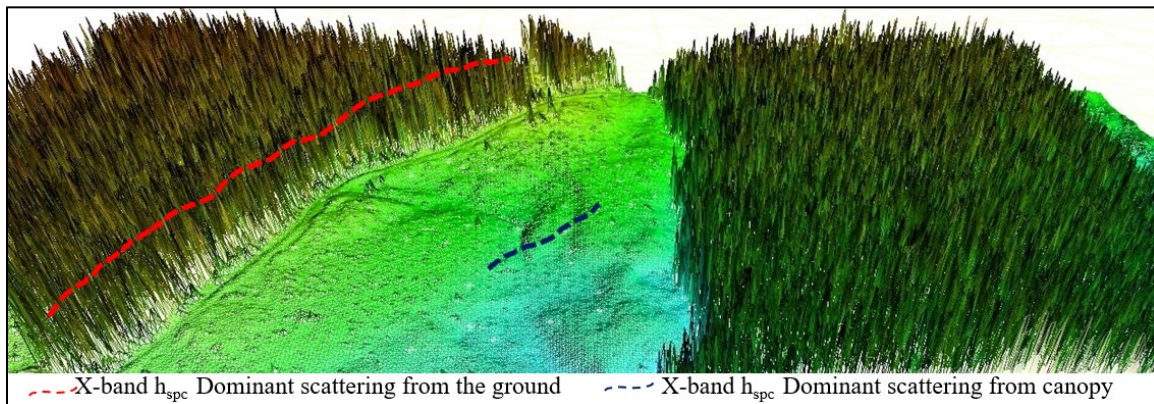


**Figure 7.8. Relative position of X-Band IfSAR  $h_{\text{spc}}$  for bare ground (blue dashed line) and over dense forest (red-dashed line). The data presented in this illustration represents the DSM lidar data over a section of Edson, Alberta, Canada [Tighe, 2012].**

Generally, the main **scattering elements** tend to be of comparable size to the wavelength of the radiation (X- ( $\lambda = 2.4$  to  $3.75$  cm) and C-band ( $\lambda = 3.75$ - $7.5$  cm) energy, while tree trunks and the ground surface will act as strong scatterers at L-band ( $\lambda = 15$ - $30$  cm) and P-band ( $\lambda = 30$  cm to  $120$  cm), all else being equal (e.g., density, cover type, **incidence angle**, polarization, etc.). Moreover, the penetration depth of the microwave signal into porous medium increases from K-band ( $\lambda = 1.13$  cm to  $1.66$  cm) through P-band or with increasing wavelength (Figure 7.9). For example, the DSM IfSAR height for X-/C-band short wavelength IfSAR may be in the upper part of a forest canopy and can be used directly as a rough estimate of canopy height [Andersen et al., 2008]. Conversely, longer wavelengths (such as L- and P-band) penetrate deeper, interacting with the ground, tree trunks, and other lower canopy elements, depending on the characteristics of the canopy, and can provide rough estimates of bare ground surface elevation.

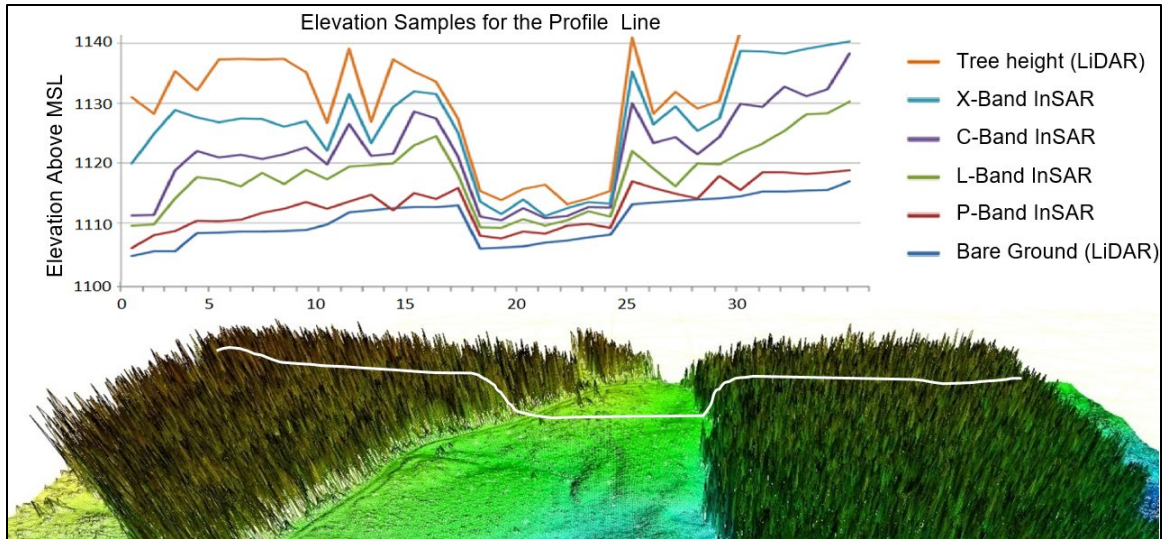


**Figure 7.9. IfSAR signal penetration over dense vegetation and bare ground at different wavelengths for a profile line in grey, superimposed on a lidar DSM [Tighe, 2012].**

Ideally, the choice of wavelength would be tailored to electromagnetic properties of the surface of interest. However, the varied nature of the Earth’s terrain precludes any single frequency from satisfying all possible application requirements. For example, SAR signal penetration depth within vegetation varies with wavelength as follows: 1-7 m at X-band, 3-10 m at C-band, 3-15 m at L-band, and 7-35 m at P-band [Lewis and Henderson, 1999]. In sparse vegetation canopies, all wavelengths will produce signal returns from the ground and lower canopy elements, resulting in a lower overall scattering phase center height, that which is closer to bare ground elevations. One estimate or the other may be more desirable depending on the application. For repeat-pass interferometry topographic systems, shorter wavelength systems are usually preferred because temporal decorrelation is less than for higher frequency systems, particularly in vegetated regions.

Electrical composition of a surface is characterized by its dielectric constant. The dielectric constant of a material determines how much energy is absorbed or reflected from the surface and depends on the radar frequency. Surface structure is usually characterized by roughness, a measure of how much the surface varies in a resolution element. Roughness is measured in terms of the incident radiation’s wavelength, so surfaces that are smooth at one wavelength may appear rough at another wavelength. As a rule of thumb, the rougher the surface the greater the backscatter.

Surface variations on the order magnitude of the radar wavelength will scatter radar as specified by the Rayleigh criterion. The Rayleigh criterion can be used to differentiate between, for example, surface topography in non-vegetated areas or extent of vegetation in others. The Rayleigh criterion defines a surface as smooth if  $h$  (in equation 7.7) is less than 1/8th the radar wavelength [Balmer and Hartl, 1998]:

$$h = \frac{\lambda}{8 \sin \theta} \tag{7.7}$$

Where:

- $h$  surface roughness, defined as the root-mean-square (RMS) height relative to a perfectly smooth surface,
- $\lambda$  wavelength of the SAR
- $\theta$  incidence angle

Horizontal smooth surfaces such as calm water reflect nearly all incident energy away from the radar antenna (called **specular reflection**) at the same angle as the **incidence angle** per **Snell's law** (Figure 7.10 – specular reflection) returning little to no signal back to the SAR receiver and resulting in a dark image tone or decorrelation in phase. In contrast, microwaves incident upon a rough surface are scattered in many directions (called diffuse scattering/reflectance).

Reflections can bounce again off other objects and be redirected back toward the SAR receiver, resulting in a stronger return signal (Figure 7. 10 - **volume scattering** and **dihedral reflection**). In the case of volume scattering, which occurs in vegetation where (high water content) leaves reflect radar signals onto other leaves and branches, multiple scattering occurs until the signal exits the vegetation. A percentage of the incoming radar is therefore volumetrically scattered back to the SAR sensor, giving the vegetation a brighter signature than a smooth lake.

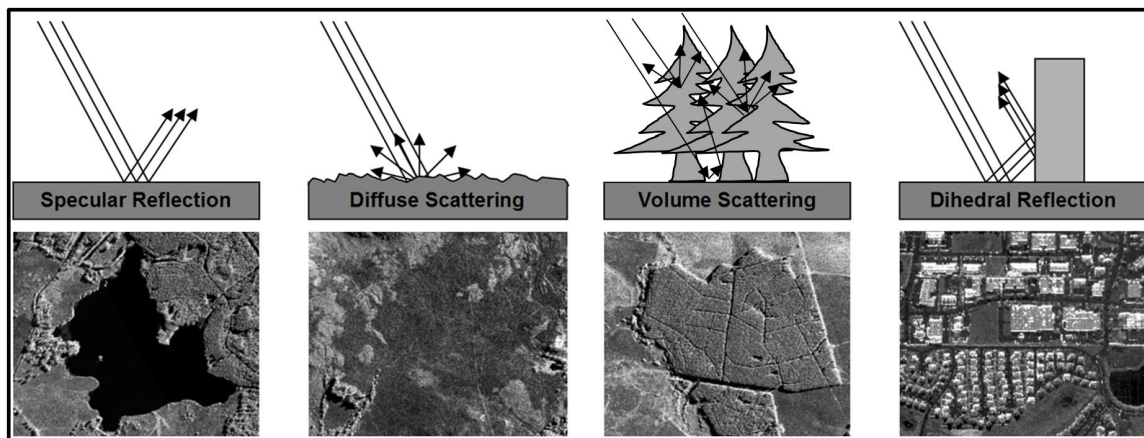


Figure 7.10. Surface roughness effects on radar backscatter for four land cover types. L-R: a body of calm water (specular reflection), grass (diffuse scattering), forest (volume scattering), and buildings.

### IfSAR Sensor **Viewing Geometry**

IfSAR configurations use oblique side looking viewing geometry that can lead to distortions in the SAR Imagery and derived elevations. Unlike some optical sensors that look directly below the imaging platform, radar and IfSAR sensors “view” the ground per a perspective beam that looks out to the side of the platform (Figure 7.11).

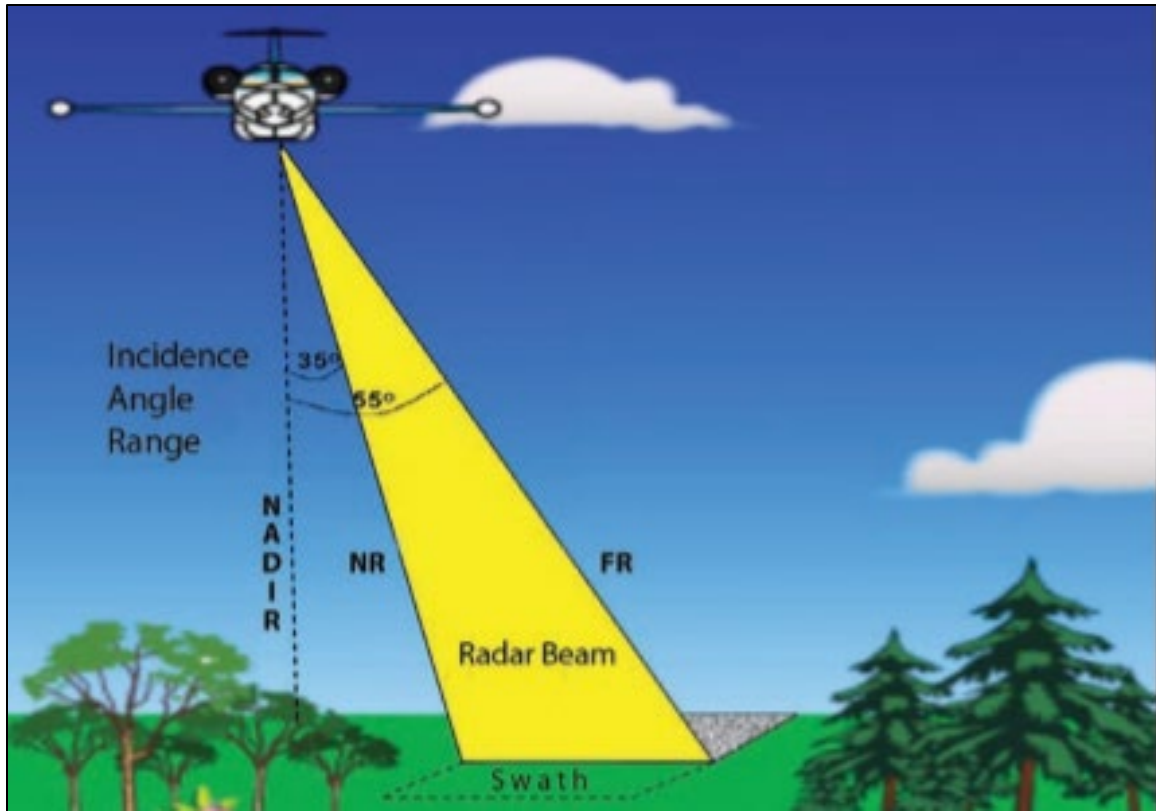


Figure 7.11. Figure showing the side looking viewing geometry of an IfSAR system in which the radar beam (in yellow) has an **incidence angle** range from  $35^\circ$  to  $55^\circ$ . The location of the **near range (NR)** and **far range (FR)** and swath width are also indicated.

The beam shown in yellow in Figure 7.11 corresponds to the line between the radar antenna and the target on the ground. The radar sensor points the radar beam out to one side of the aircraft, defining an **incidence angle** range. This configuration is an optimized viewing geometry for an IfSAR topographic mapping system. As the aircraft (or spaceborne system) flies over the terrain, an image strip or swath is collected. This beam, called the **slant range**, is the distance as measured by the radar directly, in effect along each line perpendicular to the flight vector and directly with the radar and each scatter. The slant range is further defined by two terms: **near range (NR)** and **far range (FR)**. A target located in the NR is closer to the antenna than a target positioned in the FR location. This viewing geometry creates distortions radiating out from the NR to the FR, rather than radiating out from nadir, as with aerial photography data collections.

### **SAR Image Distortion**

Because the range direction is not parallel to ground coordinates, SAR images are distorted relative to a planimetric view. Three common distortion phenomena observed in SAR imagery that bear mention are foreshortening, layover and shadow, shown in Figure 7.12.

**Foreshortening** in radar imagery results from the fact that relief displacement is towards the direction of the radar. Because the range increases more slowly than ground coordinates on slopes facing toward the radar (higher elevations contend with increasing ground distance, slowing the range increase) they tend to appear bunched relative to a planimetric view. The opposite occurs on slopes facing away from the radar (lower

elevations coupled with increasing ground distance speeds the range increase) where they tend to expand out when compared to a planimetric view Both situations are illustrated in Figure 7.12. Note that foreshortening in radar images is opposite to that of optical imagery where relief displacement is away from the direction of the camera.

**Layover** is a limiting case of foreshortening where points arranged with increasing ground coordinates appear reversed in the radar imagery. Layover occurs because the range to objects with larger ground coordinates is less than the range to other objects with smaller ground coordinates. Geometrically this happens when the slope of the terrain is greater than the angle the incident radiation makes with respect to vertical. More importantly for our purposes is to note for interferometric radar systems layover causes a loss of useful signal and therefore precludes the determination of elevation in layover regions.

**Shadow** occurs when the radar beam cannot reach a portion of the terrain being imaged because it is occluded by other parts of the terrain or other objects in the scene. Where the terrain is shadowed the radar, image will appear dark and the signal to these range cells is only due to thermal noise. As with layover regions, shadowed regions have no useful interferometric signal and consequently no elevation values can be determined.

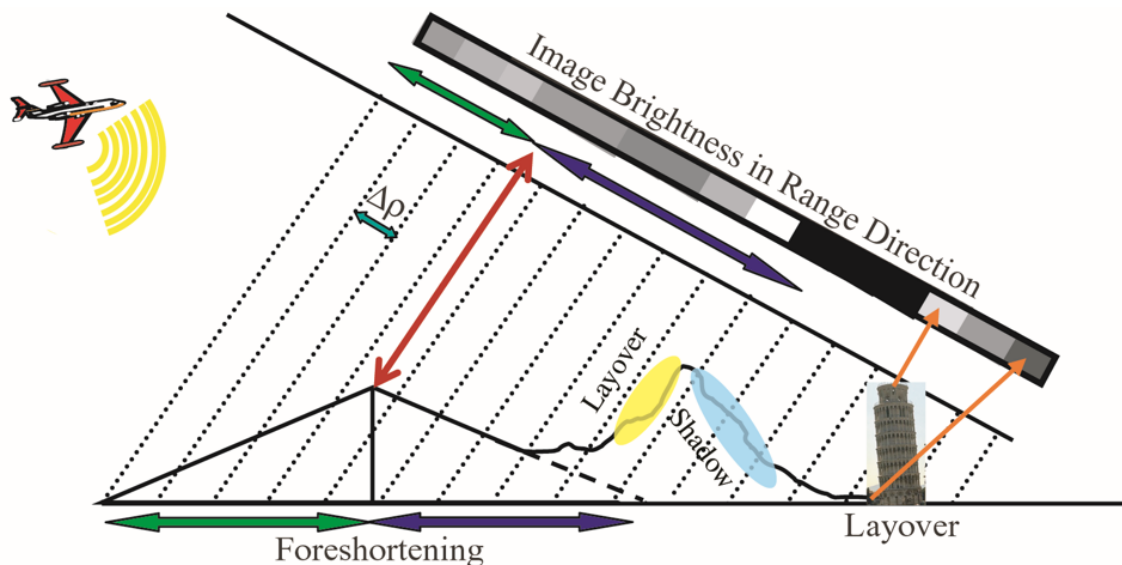


Figure 7.12. The three-dimensional world is collapsed to two dimensions in conventional SAR imaging. After image formation, the radar return is resolved into an image in **range-azimuth coordinates**. This figure shows a profile of the terrain at constant azimuth, with the radar flight track into the page.

IfSAR systems, being able to resolve the three-dimensional coordinates of points in SAR imagery, can produce imagery having correct planimetric placement in regions where there are good interferometric phase measurements.

### **IfSAR DEM Distortion**

The side looking IfSAR sensor configuration maps a look or **incidence angle** range ( $\theta$  – Figure 7.2) away from nadir. **Incidence angle range** is arbitrarily denoted as **near-range (NR)**; closest to nadir; or steep – Figure 7.12)), **mid-range (MR)**, or moderated – Figure 7.12), and **far-range (FR)**; furthest from nadir; shallow – Figure 7.12) across a flight line strip of data or an orbital pass. Incidence angle variations across the swath are usually more pronounced in airborne data collections and result in variations in varying relative signal contributions from ground and surface features as illustrated in Figure 7.13. The resulting

elevation measurements as described earlier reflects this relative signal strength of the various scattering elements and therefore the vertical location within the medium for which the elevation corresponds.

In airborne collections, for example, at steep **incidence angles** (e.g. NR –  $\theta \sim 35^\circ$ ; Figure 7.13, left-hand tree) more exposure of the lower portion of a vegetation canopy and ground occurs because of greater signal penetration into the canopy, resulting in a  $h_{\text{spc}}$  or estimated elevation height that is closer to the ground elevation [Hensley et al 2001, Andersen et al., 2005; 2008, Garestier et al, 2008, Hajnsek et al 2008, Tighe et al, 2012]. The opposite effect occurs for the same tree located, in the FR (e.g. NR –  $\theta \sim 55^\circ$ ; Figure 7.13, right-hand tree) such that the  $h_{\text{spc}}$  or estimated elevation height that is closer to the top of the tree canopy elevation. Interferometric mapping systems can reduce the impact of **incidence angle** sensitivity by combining multiple flight lines strips of data.

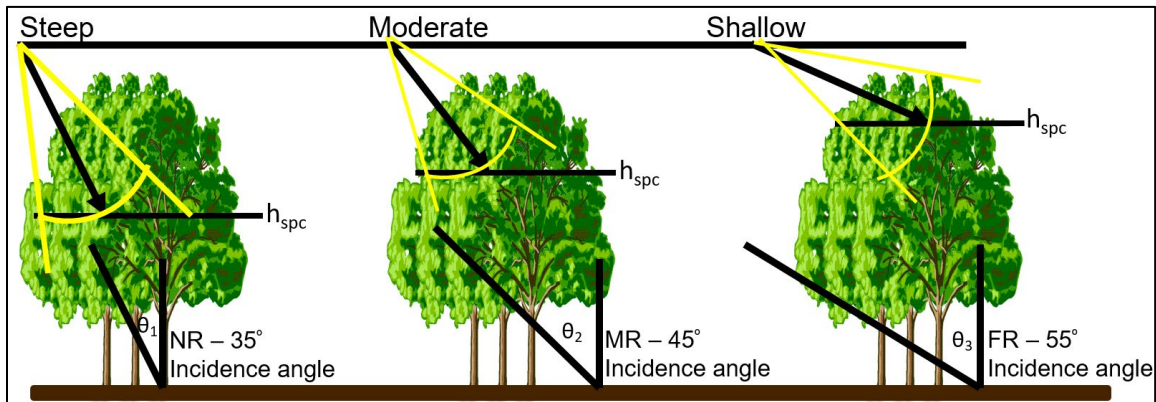


Figure 7.13. **Incidence angle** effect on  $h_{\text{spc}}$  retrieval of surface elevation data for single-pass IfSAR.

Because radar primarily interacts with structures that have lengths comparable to the wavelength or larger, longer wavelength radars tend to penetrate deeper into the vegetation canopy or ground surface. The amount of penetration in a vegetation canopy, bare ground or snow or ice layers depends on the structure of the scattering medium as described earlier. Radar wavelengths less than roughly 10 cm mostly sense the upper portions of canopies while wavelengths longer than 20 cm sense deeper into a canopy. Longer wavelength radars have been known to penetrate several meters or more in dry sandy soil and even deeper into certain types of ice (10s of meters). Commercial IfSAR providers attempt to minimize this effect by processing and averaging several data collections (Figure 7.14) or using systems designed specifically to compensate or minimize this effect.

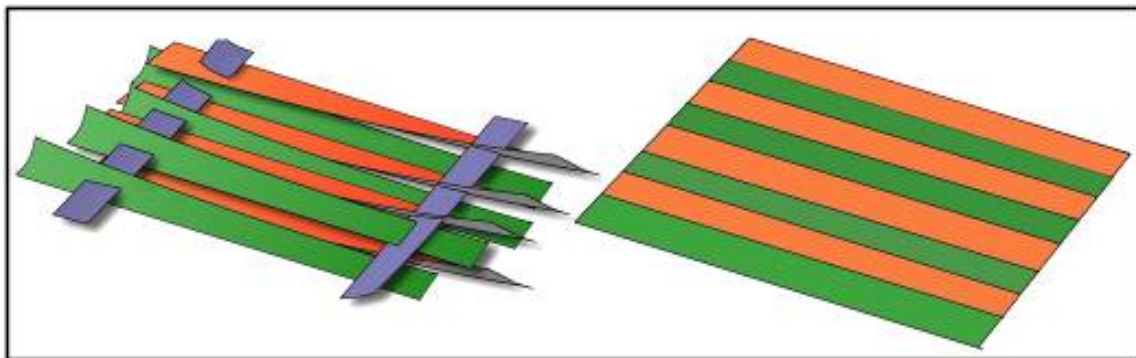


Figure 7.14. Example of airborne IfSAR strip DSM data collection merging of primary (green and

orange single take data strips) and tie (blue single take strips) flight line strips that are merged to derive the final DSM given in the right mosaic.

## DEVELOPMENTAL HISTORY

The IfSAR mapping for Earth based topography measurement had its genesis with an airborne SAR system by Graham in the early 1970's [Graham, 1974]. Later IfSAR techniques for non-military applications was undertaken by various groups including the U.S. Jet Propulsion Laboratory (JPL), the Canada Centre for Remote Sensing (CCRS), the Environmental Research Institute of Michigan (ERIM), European Space Agency (ESA), German Aerospace Centre (DLR), and others. These investigations utilized airborne platforms including the CCRS CV-580, the JPL DC-8, and space platforms, such as SEASAT, European Remote Sensing-1/2 (ERS), and the space shuttle Shuttle Imaging Radar-A to -C (SIR-A-C) radars. In 1996, Intermap Inc. fielded the world's first commercial implementation of a high-performance airborne interferometer, called STAR-3i whose development was funded by DARPA and used algorithms developed by the Jet Propulsion Laboratory. There have been many spaceborne SAR instruments flown in recent decades: ERS-1/-2 and ENVISAT satellites operated by the European Space Agency, JERS-1 and ALOS PALSAR operated by the National Space Development Agency of Japan, RADARSAT-1 and -2 operated by the Canadian Space Agency, SIR-C/X-SAR operated by the United States, German, and Italian space agencies, TerraSAR-X and Tandem-X operated by Airbus and the Italian Cosmo/SkyMed operated by the Italian space agency. SAR constellations such as Copernicus (C-band) and urthecast along with spaceborne SAR instruments like the NASA/ISRO NISAR (L and S-bands), European BIOMASS (P-band), German/Brazilian MAPSAR (L-Band), and Japanese ALOS II (L-band) and will continue to spawn new IfSAR technology and applications. Commercially available IfSAR systems are detailed in the IfSAR operation sensors section found in this chapter.

## IfSAR DEM MAPPING CONSIDERATIONS

When considering the acquisition of IfSAR generated DEMs or IfSAR data to generate DEMs, the following key IfSAR mapping considerations should be considered. Constructing accurate DEMs using radar interferometry requires precise knowledge of the IfSAR sensor platform position, attitude, and interferometric baseline as well as knowledge of the radar operating parameters. Phase stability and tracking of any phase changes not a result of topographic variations are also key considerations for IfSAR mapping systems. Here we outline elements common to all interferometric mapping systems and describe some of the tradeoffs between the various configurations. This treatment is geared for DEM users who need to understand how best to select a system that accommodates their mapping requirements.

### ***IfSAR Sensor Configuration***

There are two standard approaches to obtain the two SAR images necessary for IfSAR topographic elevation mapping: 1) single-pass interferometry (SPI) and 2) repeat-pass interferometry (RPI) illustrated in Figure 7.15.

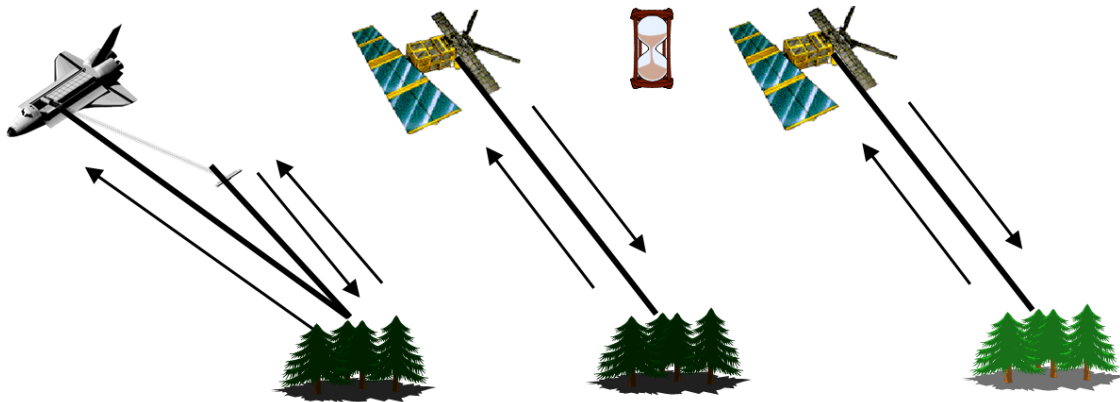


Figure 7.15. Interferometric radar topographic measurements are made with **single-pass (SPI)** and **repeat-pass (RPI)** systems. SPI configuration consists of two spatially separated antennas (usually on the same platform) arranged to collect echoes from the terrain simultaneously (left image - the **SRTM** mapping IfSAR with two antennas separated by a 60-m retractable boom (interferometric baseline). In RPI (middle and right images), the scene is imaged at least twice separated by an interval of time that may be seconds to years.

SPI configurations occur when interferometric observations are made with both antennas on the same platform<sup>3</sup>. In the case of RPI multiple observations are separated in time. RPI observations may be separated by as little as a fraction of a second or may be many years apart.

RPI is possible when the flight tracks are separated by less than the critical baseline length and when the surface has not changed enough to cause decorrelation. The time lapse between the two acquisitions creates a temporal interferometric baseline which typically ranges from minutes (for airborne systems) to many days (even years) representing the repeat orbit period of the satellite (e.g., 24 days for RADARSAT). Atmospheric changes between observations, particularly those attributed to tropospheric water vapor, can dramatically alter **interferometric phase measurements** [Goldstein, 1995], [Zebker et al, 1997]. Spatial scales for **atmospheric phase distortion** effects are typically on the order of kilometers and scale in direct proportion to wavelength. The effect on interferometric height measurements can be a meter to hundreds of meters depending on the amount of distortion and the baseline length. Spaceborne SARs flying above the ionosphere (orbits above 300 km) also experience **phase distortions** due to changes in the ionosphere between repeat observations, however these changes typically have larger spatial scales of 10-100 kilometers and have a non-linear wavelength dependency. The non-linear wavelength dependence offers the possibility of removing **ionospheric distortion** by flying a multi-frequency system, like the way GPS corrects for the ionosphere using two frequencies.

IfSAR systems grouped by the platform type, airborne or spaceborne, and method of data collection, single-pass or repeat-pass, yields four major implementations (Table 7.2) with various relative strengths and weaknesses.

Table 7.2. Summary of Types of IfSAR Sensors

Single Pass	Repeat Pass
-------------	-------------

<sup>3</sup> In principle, the antennas could be on separate platforms flying in formation [Zebker et al, 1994].

<b>Airborne</b>	Regional Coverage Affordable Fine Resolution Necessary Motion Compensation Benign Atmospheric Effects No Temporal Decorrelation No Ionospheric Effects Possible Need for Active Baseline Metrology	Regional Coverage Affordable Fine Resolution Necessary Motion Compensation Problematic Atmospheric Effects Temporal Decorrelation Effects No Ionospheric Effects Difficult Track Repeatability Difficult Baseline Estimation Change Detection Possible Increased Baseline Flexibility
<b>Spaceborne</b>	Global Coverage Costly Fine Resolution Benign Motion Compensation Benign Atmospheric Effects No Temporal Decorrelation Problematic Ionospheric Effects Baseline Metrology Required	Regional Coverage Costly Fine Resolution Benign Motion Compensation Problematic Atmospheric Effects Temporal Decorrelation Effects Problematic Ionospheric Effects Difficult Track Repeatability Benign Baseline Estimation Change Detection Possible

### **Airborne Single Pass Interferometry (SPI)**

Single pass aircraft systems (e.g. **STAR** and **GeoSAR**) are well suited for generating fine resolution regional scale DEMs. Single pass systems are best suited for generating high quality topographic maps to a specified absolute accuracy since they do not suffer from temporal decorrelation or from atmospheric phase distortion problems. Aircraft systems have a great deal of flexibility in scheduling data acquisitions, orientation of flight lines, and modes of operation.

### **Spaceborne Single Pass Interferometry (SPI)**

Spaceborne platforms have the advantage of global and rapid coverage and accessibility. Increased coverage for spaceborne systems comes about from the combination of the faster velocity by a factor of 30 and the larger swath widths ranging from 50-500 km. Spaceborne systems also avoid airspace restrictions that make aircraft operations difficult in certain parts of the world. Typical baselines for spaceborne IfSAR system making topography measurements range from 10-1000 meters. This poses a difficult metrology problem regardless of whether the antennas are connected to the same platform or are on separate platforms flying in formation. Tracking phase instability of the radar hardware and antennas, which may go through a hundred degrees Celsius or more of temperature change in an orbital period, requires special hardware. **SRTM** and Airbus's **Tandem-X** satellites are the only spaceborne single-pass IfSAR systems flown to date.

### **Spaceborne-Repeat Pass Interferometry (RPI)**

Repeat pass interferometric observations have their greatest utility in measuring surface deformation over wide areas for geophysical applications such as earthquake monitoring, volcano inflation and deflation, and glacier motion rather than topographic elevations. Nonetheless, repeat pass IfSAR (e.g. **RADARSAT-1/2**, **TerraSAR-X** and **COSMO SkyMed**) has been used to make topographic maps in many parts of the world, often exceeding the accuracy of the best topographic maps currently available in those regions.

Besides tropospheric or ionospheric propagation effects to the interferometric phase (explained in detail in previous DEM User Manuals), the other major limiting factor to repeat-pass IfSAR topographic map generation is **temporal decorrelation**.

### **Polarimetric-Interferometric SAR (PolInSAR)**

Another IfSAR sensor configuration called PolInSAR combines polarimetry (defined below) and IfSAR to derive bare ground elevations and canopy height measurements. **Polarimetry** deals with the full vector nature of polarized (vector) electromagnetic waves throughout the frequency spectrum from Ultra-Low-Frequencies (ULF) to above the Far-Ultra-Violet (FUV) [Boerner et al., 1998]. A complete description of radar polarimetry is beyond the scope of this chapter; however, we mention a few relevant aspects about radar polarization are needed for our heuristic development **polarimetric interferometry**. The electric and magnetic fields comprising an electromagnetic wave are vector quantities meaning they have both a magnitude and direction (Figure 7.16). The vector nature of electromagnetic radiation gives rise to sensitivity to the orientation of an object from which it scatters and hence provides additional information about the scatterer.

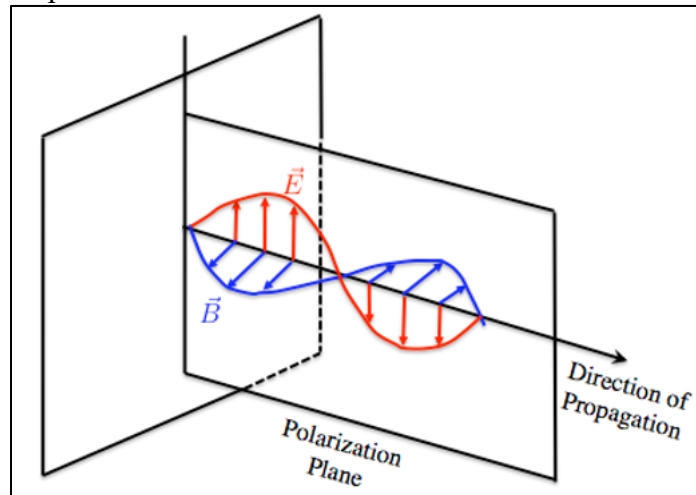
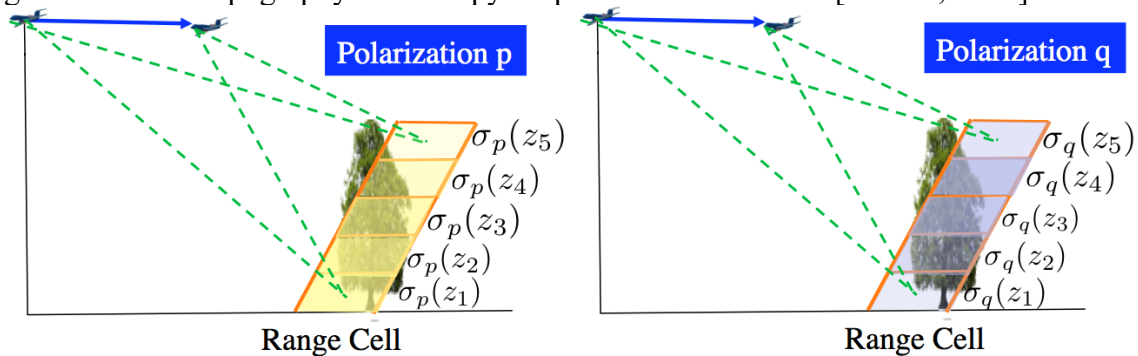


Figure 7.16 The direction of the electric field (and the magnetic field) lies in the plane perpendicular to the direction of propagation and defines the polarization of the wave.

**Microwave polarization** is characterized by the shape of the path that the electric field vector traces out in the plane perpendicular to the direction of propagation. The most general path is an ellipse that can be characterized by two parameters. Tilt measures the orientation of the ellipse with respect to the horizontal direction and **ellipticity** is a measure of the amount of deviation from a circular shape. Now although there are an infinite number of polarization states, it turns out that by transmitting and receiving data on two suitably chosen polarizations (a sufficient requirement is that they be orthogonal) it is possible to synthesize all other polarizations from a combination of these representative polarizations. The most common representative set used by most radars are **horizontal polarization** and **vertical polarization** denoted by H and V respectively. Polarimetric radars operate by transmitting H and V polarization on alternate pulses and receiving both H and V polarization on every pulse. Radars can also operate in restricted polarization combinations, say transmitting only H and receiving H and V or transmitting H and receiving H and transmitting V and receiving V. When the sensor is operated in a restricted polarization combination it is not possible to synthesize all possible polarizations any

longer. The amount of **backscatter** depends on polarization because it is sensitive to the orientation of scatterers within a resolution element. Polarization diversity can also be used to identify dominant scattering mechanisms within a resolution element as well as determine quantitative information about the orientation of objects.

Collecting polarimetric data from two spatially separated SAR antennas generates scattering diversity that can be exploited to solve for information about the volume. Figure 7.17 illustrates polarimetric interferometric returns from two polarizations for the same resolution element. Note, the backscatter magnitude variation as a function of height in the volume and is different for the two polarizations and hence the **volumetric correlation** is different for different polarizations. Using models such as the **random volume over ground (RVoG)** or **polarization coherence tomography (PCT)** information about vegetation height, ground surface topography and canopy shape can be ascertained [Cloude, 2010].



**Figure 7.17 Different polarizations backscatter differently as a function of height within a canopy and hence additional information on the structure of the volume can be obtained using **polarimetric interferometry**.**

The power of the **PolInSAR** technique is best illustrated with a tree example, Figure 7.18. A tree contained within a single resolution element, highlighted in shades of yellow in Figure 7.18, is imaged from two vantage points separated by an **interferometric baseline** shown in blue. The various shades of yellow show the amount of backscattered energy that varies depending on height within the canopy, e.g., thicker portions of the canopy in the intermediate heights may scatter more than sparse vegetation as the top of the canopy. Recall, that the interferometric phase is proportional to the differential path length from the two antennas which is illustrated in red,  $D_b$ , for the bottom of the canopy and in orange,  $D_t$ , for the top of the canopy.

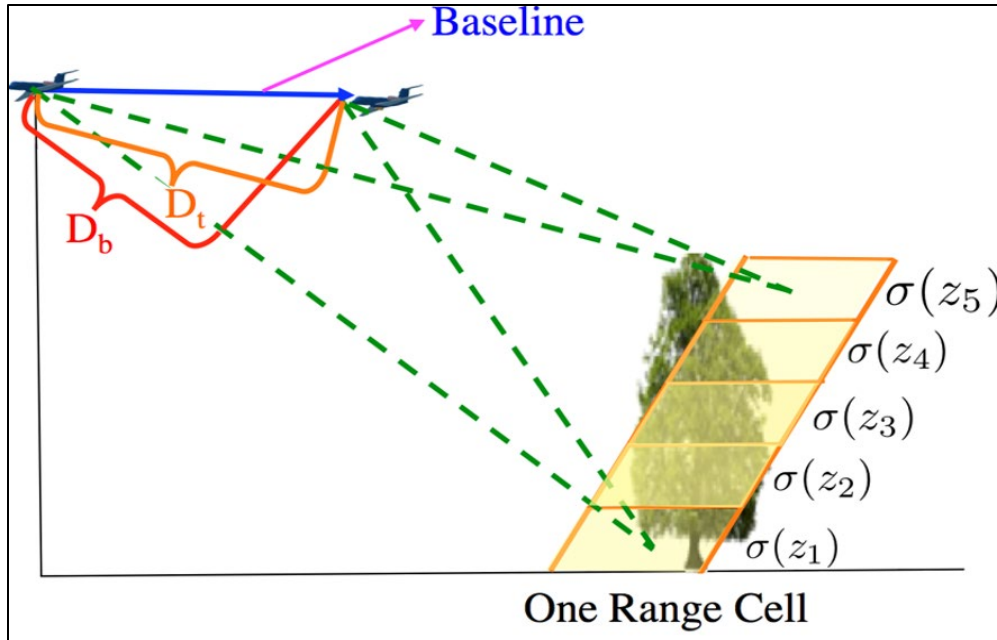


Figure 7.18. A tree contained within a single radar resolution cell is imaged from two vantages separated by a baseline shown in blue. The amount of **backscatter** signal and phase are a function of height within the tree.

Because the differential path lengths are varying as a function of height within the canopy so is the **interferometric phase**. Note, if the baseline length goes to zero then the path lengths are identical regardless of location within the canopy and there is no interferometric sensitivity to the volume. The interferometric signal from a resolution element is a backscatter weighted combination with phase varying as a function of height to the canopy elements contained in the cell. Thus, radar interferometry has sensitivity to the volume but with only one observation per resolution element has limited visibility to the internal structure within a range cell.

We see that interferometric measurements from a resolution element essentially consists of two components: first, a scattering component that depends on the strength of the reflected signal that varies as a function of height within a resolution element, and second a geometric component that depends on the interferometric baseline and determines how quickly the **interferometric phase** varies as a function of height within a resolution element. Thus, to obtain additional information about the vertical structure within a resolution element we need to either increase scattering diversity or the **geometric diversity**. Increasing geometric diversity is accomplished by imaging the scene with multiple baselines. If enough multi-baseline observations are made it is then possible to use tomographic imaging techniques to get fine vertical resolution information of the backscatter. Alternatively, one can obtain **backscatter diversity** by varying the polarization of the electromagnetic radiation.

We present an example using data from the NASA/JPL L-band UAVSAR radar system collected in La Amistad National Park, Costa Rica in February of 2010 [Hensley et al., 2014]. **UAVSAR** is a NASA/JPL L-band fully polarimetric synthetic aperture radar employing an electronically scanned array whose primary design goal was to enable robust repeat pass radar interferometric measurements of deforming surfaces either from natural or anthropogenic causes. The radar is housed in a pod mounted to the fuselage of a

Gulfstream III jet. Nominally, the aircraft flies at an altitude of 12.5 km and maps a 22-km swath with incidence angles ranging from 25° to 60°. The 80 MHz range bandwidth results in single look complex (SLC) imagery with range and azimuth resolutions of 1.66 m and 1 m respectively. Electronic steering of the antenna is tied to the inertial navigation unit so that consistent pointing is achieved regardless of the platform yaw. The platform was modified to include a platform precision autopilot (PPA) that allows the aircraft to fly a specified trajectory within a 5-m tube. This enables UAVSAR platform to fly a series of flight lines with well prescribed interferometric baselines.

On February 8, 2010 UAVSAR collected a series of repeat pass lines with a variety of physical baselines. Data were collected from coast to coast to cover a wide range of biomes and terrains. Figure 7.19 shows polarimetric radar imagery and a multi-color correlation image for a site in La Amistad National Park. Flat open areas have high correlations as shown in the right image as there is no volumetric correlation whereas forested areas exhibit lower correlations depending on the amount of volumetric correlation at that polarization. In addition to the volumetric correlation because the data were collected in a repeat pass mode there is also temporal decorrelation. The smaller the physical baseline the bigger the impact temporal decorrelation has on tree height estimate. Temporal decorrelation biases tree height estimates high. Several methods have been proposed to mitigate the impacts of temporal decorrelation, however their efficacy is situation dependent.

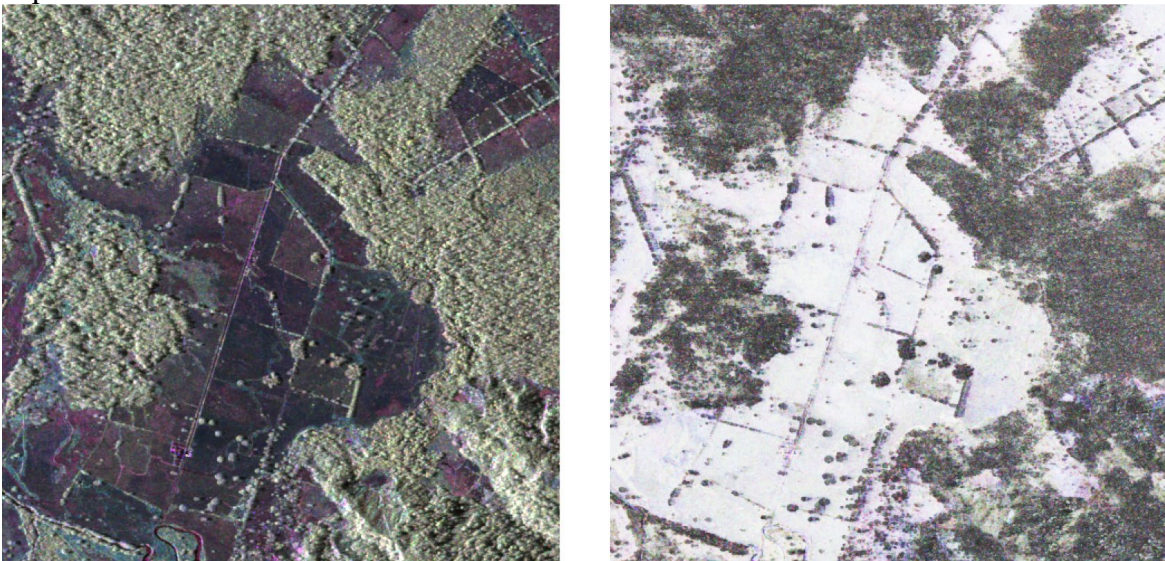


Figure 7.19. Polarimetric imagery and interferometric correlations for a selected portion of the La Amistad National Park. Blue denotes hh+vv, red hh-vv and green is hv collected on February 8, 2010.

Figure 7.20 shows tree height estimates for 6 physical/temporal baseline combinations. Physical baselines varied from 60-100 m and the temporal baselines varied from 0.7-1.9 hrs. The tree height estimates are very similar, except for Baseline 5 (60 m, 0.7 hr) which is biased high compared to the other estimations. This is because Baseline 5 has the smallest baseline, making it more sensitive to temporal correlation (that degraded the tree height estimates).

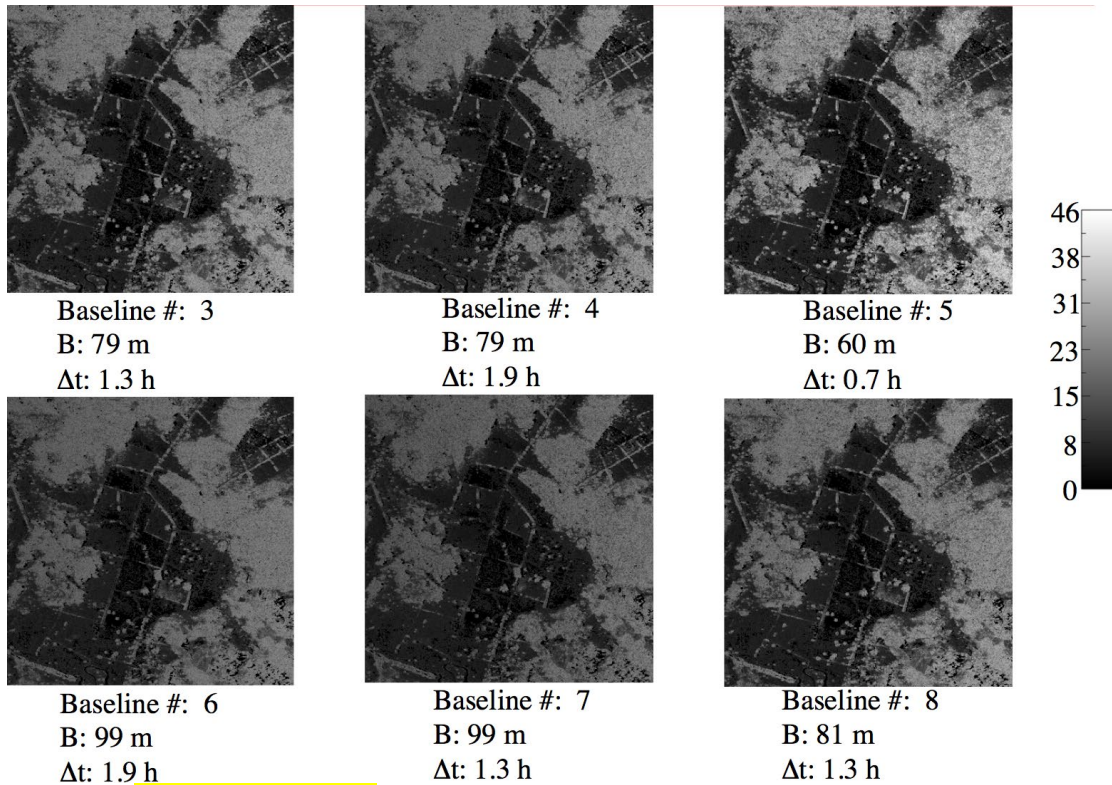


Figure 7.20: **Tree height estimates** for 6 spatial/temporal baseline combinations. Tree height estimates are very similar except for Baseline 5 where increased **temporal decorrelation** results in increased tree heights.

Figure 7.21 shows histograms of the tree estimates. The histogram of Baseline 5 is the yellow curve that has an extended tail for larger tree heights that is a result of the increased impact of temporal decorrelation.

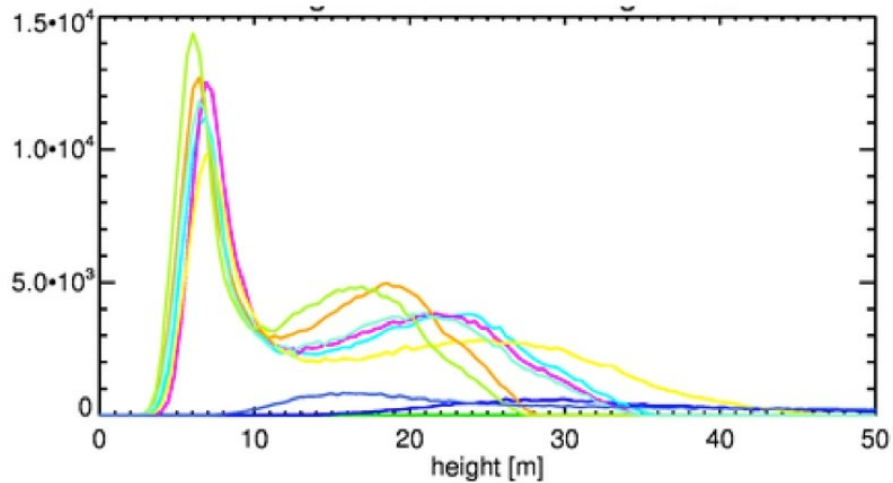


Figure 7.21: **Histogram** of the **tree height estimate** for the 6 spatial/temporal baselines. The yellow line corresponds to the histogram of the baseline which has an extended in tail for larger tree heights resulting from the increased effect of temporal correlation.

### Platform Position

While it is straightforward to measure distances (e.g. phase information needed to derive topographic height measurements) using IfSAR techniques, precise knowledge of the

location of the SAR antennas is required, consequently requiring the need of two additional technologies GPS (or **Global Navigation Satellite System -- GNSS**) and **inertial navigation system (INS)**, explained in Chapter 12. Position measurement with the advent of GPS and differential GPS (DGPS) systems are very good; INSs enables very accurate motion measurement on a broad range of time scales. Kinematic GPS used with either airborne or spaceborne platforms achieves decimeter absolute position accuracy with a 2 Hz sampling rate. Although 2 Hz sampling of the motion works for satellites that have relatively smooth trajectories, faster sampling of 20 Hz or greater is required for airborne IfSAR applications. Inertial measurement unit (IMU) systems provide the faster motion and attitude update rates needed for motion compensation. Blending of kinematic DGPS and IMU data is an increasingly common method of optimizing position and attitude data to have a high effective sampling rate and excellent absolute position accuracy necessary for airborne and spaceborne applications.

For interferometric applications, it is knowledge of the antenna locations that is essential and required for baseline determination and motion compensation. Rarely are the motion metrology systems mounted to the center of the antenna; therefore, platform attitude measurements coupled with measurements of the antenna location relative to the motion sensors is needed. Absolute angle determination with accuracy of approximately a few thousandths of a degree is off-the-shelf technology today with tightly coupled IMU/GPS systems, significantly improving the critical determination of the baseline orientation angle. For spaceborne platforms, star trackers provide absolute attitude measurements with 1-10 arc second accuracy. If faster update rates are needed, then star tracker measurements are coupled with IMU measurements.

It is not always possible to design IfSAR systems such that the antennas remain fixed relative to the motion measurement system. When this is the case additional metrology devices are required to track antenna motion with respect to the platform. Very few systems thus far have been fitted with active baseline metrology systems but those that have used a combination of optical ranging and target tracking devices. Update rates for these systems are matched to the expected motion of the antenna relative to the platform to insure proper baseline determination.

Spaceborne radars, until recently, have relied upon **Doppler tracking** for orbit determination. Doppler tracking can determine satellite positions with accuracy from 10 cm to 100 m depending on the orbit and the amount of tracking data available. The highest accuracy Doppler derived orbit position data may fall short of the accuracy requirements needed for repeat pass interferometry (RPI) topographic mapping. Almost all modern spaceborne radar systems are equipped with GPS receivers, vastly improving the orbit determination. Orbital positions with a 3-10 cm accuracy are routine. For those baselines that must be known to a centimeter or even sub-centimeter accuracy cannot be determined strictly using Doppler tracking data. Ground truth in the form of existing DEMs or radar identifiable ground control points are used to determine the baseline for RPI topographic applications when adequate metrology is not available.

### **Platform Calibration**

IfSAR data collection systems are operated in a similar manner to other survey sensors. Sensor error models are created through a calibration process and used within a production

process. Further, data acquisition includes the collection of redundant data that are used to validate and if necessary refine the calibration parameters.

**IfSAR calibration** is a process with a goal that is not unlike the concept of calibrating a photogrammetry camera. As with these metric cameras and their **interior orientation parameters** (focal length, lens model, and perspective center offset), IfSAR sensors require an understanding of certain physical behaviors – primarily timing and impulse response of the transmitted SAR signals. As is the case in photogrammetry, calibrating cameras utilizing the co-linearity equations, IfSAR systems utilize a set of performance equations based on equations that determine a scatterer’s location from the interferometric observables. With a calibrated IfSAR system, a similar collection strategy to photogrammetry is typically utilized. Thus, one of the keys to acquiring accurate and reliable terrain elevation data from IfSAR platforms lie in the knowledge of the radar antenna locations essential for interferometric baseline determination and motion compensation.

The concept of tie point and ground control point used in block adjustments are employed as “parallel profiles”, tie lines, and ground control points. These are used to establish the equivalent of the **exterior orientation parameters** for each flight. The ultimate accuracy budget for the IfSAR is then based on a fully calibrated sensor with a loosely coupled navigation solution combining GPS and INS streams, all measured and controlled by profiles and control points. The IfSAR product vertical accuracy has been tested and independently verified many times and consistently achieves 3 m vertical RMSE for the DEMs in low slope unobstructed areas, and 3 m CE95 for the ORIs without the use of in-scene ground control. Note, the height precision for IfSAR mapping systems is often considerably better than the height accuracy.

## **IF SAR DATA POST PROCESSING**

Processing and post processing of IfSAR data to derive commercial DEMs (DSM and DTM) affect the accuracy and quality of final map products. The division between processing and post processing is somewhat arbitrary, however for the purposes of this chapter post processing will be defined to begin after the interferometric phase is transformed to a position and elevation measurement. Commercial companies utilize proprietary software to generate the digital elevation models from interferometric data. Many aspects of IfSAR post processing are like standard photogrammetric or lidar post processing. The type and amount of post processing is application dependent and is tailored to meet specific user requirements. The most common IfSAR post processing steps are described.

### **IfSAR DEM Void Fill**

Data gaps resulting from too much decorrelation, e.g., low backscatter from calm water, **layover** or **shadow** regions, may still be present after mosaicking is complete. Most commercial vendors fill these data gaps to provide fully populated DEMs. There are three basic methods used to fill gaps in the final DEM. Data may be specially acquired over the gap regions, data from alternate sources may be used, or analytical methods for filling gaps may be employed. Data from previous data collections or other data sources (e.g. USGS DEMs) may also be used to fill in gaps in the data. These data in general may not meet the same accuracy or resolution requirements of the IfSAR data, however alternate source data

often proves adequate for small gaps. By incorporating these alternate sources during the mosaicking process, a seamless final product is achieved, provided there has not been extensive change to the topography between the time of the IfSAR data collection and the time the alternate source data were acquired. Specially acquired data to fill residual gaps is the most expensive means of filling gaps in the DEM and may require a delay in product delivery to allow for data collection and processing. This option has the benefit of maintaining uniform quality data throughout the DEM but is usually only warranted when there are excessively large data voids in critical portions of the DEM. A myriad of algorithms is used to analytically fill gaps in topographic data. Surface fitting, kriging methods, and polynomial interpolators are among the most commonly employed algorithms for hole filling. The choice of algorithm depends on the size of holes to be filled and the intended application for the DEM.

### **IfSAR Data Editing**

Data editing is used to correct errors in the DEM detected during the quality control process or to manipulate height values so that they conform to a user prescribed mapping standard. **Unwrapping errors** occur when an incorrect multiple of  $2\pi$  is added to the interferometric phase measurement. This results in the IfSAR elevation measurements being too high or too low by a multiple of the ambiguity height, a quantity that is determined from the interferometric system parameters and mapping geometry. Unwrapping errors are detected and edited from the DEM by searching for height discontinuities that are multiples of the **ambiguity height**. **Spikes** and **wells** are isolated points in the DEM whose elevation differs from surrounding heights by an unphysical amount. These points are edited from the final DEM and marked as data voids or filled in using a combination of the surrounding elevation values. Some map products (e.g. DTED products) require that water bodies have single elevation value. IfSAR DEMs over water are usually noisy and have intrinsic height variation that depends on the amount of thermal noise. **Water body editing** consists of identification of the water body and setting the elevation to the desired value. Water body identification using IfSAR data is a difficult problem and is a sizable portion of the editing process.

### **IfSAR Vegetation Removal**

Applications that require bare surface DEMs (e.g. DTM) need to have IfSAR reflective surface elevation measurements corrected to bare surface elevations. Correction of reflective surface elevation measurements is called vegetation removal. Vegetation removal involves identifying vegetated regions and then correcting the elevation measurements to the bare surface. Identification of vegetated region uses combination of imagery, elevation measurements and correlation data. Correction to bare surface elevations may employ algorithms like lidar and photogrammetric sensors where elevation measurements that penetrate to the bare surface are used in combination with surface fitting algorithms to make elevation adjustments. More sophisticated algorithms that use the image brightness, correlation and elevation measurements along with a model of the vegetation are now being employed by some IfSAR sensors for vegetation removal. Additionally, polarimetric-interferometric or multiple baseline interferometry as described above can directly measure the vegetation height and used to correct the data for bare

surface elevations. Correction of IfSAR elevations to bare surface elevations in dense urban environments can be difficult.

## **IfSAR QUALITY CONTROL**

Quality control is a task or series of tasks that scrutinizes all, or a sample, of the IfSAR products issued during or at the end of the IfSAR map generation process to ensure that the final product meets or exceeds requirements. This scrutiny involves a combination of review, inspection and quantitative measurements, against well-defined criteria that are outlined in references. Additional quality controls determined by the data provider are used for other map products such as SAR imagery and other IfSAR specific derived products. Many data providers certify their QA/QC processes to the ISO standard. An overview of some of the standard qualitative and quantitative quality control procedures is presented in the following sections.

### **Visual Accuracy Checks**

**IfSAR visual quality control** begins by looking for gross processing errors associated with incomplete **phase unwrapping**, large spikes and wells, large tilts on water bodies and features that seem out of place. The maximum and minimum elevations in the IfSAR DEM are compared to the maximum and minimum values represented by contours or spot elevations available on the most recent available map. A check for completeness in the project size and for continuity along mosaic seams and data gap boundaries is also made. Overlay the IfSAR map products on available map data to check if geo-referencing is correct. Spot check selected pixel values such as corner and center pixel values against heights on published maps. Use a DEM viewing workstation with the appropriate software tools to aid in the identifications of blunders such as spikes and holes. **Blunders** are generally identified through a combination of color banding of elevation contours, stereoscopic viewing using anaglyphic filters, shaded relief enhancements and use of histograms. **Artifacts** identified during the visual accuracy checks are documented and quantified noting the location and source, for example: terrain masking, radar shadow, DEM sub-patch boundary, land/water boundary, vegetated regions, wind motion, or other factors.

### **Ground Truth**

Quantitative assessment using ground truth data is an important component of the quality control procedure. A selected set of ground control points, typically greater than 20 for any region or sub-region to be tested, is compared with the corresponding IfSAR generated height measurements. For a rectangular area that is believed to have uniform positional accuracy, check points may be distributed so that points are spread at intervals of at least 10% of the diagonal distance. At least 20% of the points are to be in each quadrant. The independent source of higher accuracy shall be of the highest accuracy feasible and practical to evaluate the accuracy of the IfSAR data. To make a rigorous accuracy assessment usually requires truth data that is three times more accurate than the product tolerance. Although vertical checkpoints are often not well-defined, each horizontal checkpoint must be well defined (see Chapter 3 of this manual, and section 7.9 of ASPRS, 2014). A well-defined point represents a feature for which the horizontal position is known to a high degree of accuracy and for which the absolute position with respect to the map

product geodetic datum is known. Kinematic GPS measurements taken along major highways and trunk roads provide excellent data sets for quality control and accuracy assessments. Kinematic GPS transects should be collected away from urban areas where multi-path in the radar and kinematic GPS data is often problematic.

Control points are usually derived from either kinematic GPS measurements or a high accuracy photogrammetric or lidar DEM with relative height accuracy at least three times better than the expected IfSAR mapping accuracy.

## **IFSAR DATA DELIVERABLES**

Data deliverables can be divided into three categories, pre-project deliverables, post-project deliverables, and map products including DEMs, imagery and other derived products. Depending on whether data is specifically collected to support a project or purchased from archived sources, not every deliverable category is applicable. The main goal of this chapter is to provide the DEM user with a list of the type of deliverables that may be available throughout the course of a project. Selection of those deliverables most useful for a project will depend on the type of data needed and the application.

## **COST CONSIDERATIONS**

As with most mapping techniques, the cost of the DEM products depends on many factors. In the case of IfSAR, some of the factors are accuracy, project size, geographic location, ground post spacing, terrain type and density, and type of the vegetation cover. Current reported prices for IfSAR generated DEMs are grouped into two categories: (1) project specific, where data is collected by the data provider to meet a specific customer mapping requirement, and (2) archival data where data is purchased from previously collected (and possibly processed) IfSAR mission data.

For project specific IfSAR, DEM prices range from \$35/km<sup>2</sup> to \$80/km<sup>2</sup> depending upon the area size, site location, terrain ruggedness, foliage density and platform. Archival data prices are lower than project specific prices and depend on whether the data must be reprocessed or can be used as previously processed. Archival data purchases are more common today with the advent of cloud storage and SaaS (Software as a Service) options. Data archive prices range from \$1/km<sup>2</sup> to \$10/km<sup>2</sup> for DEMs and typically require a minimum area purchase.

## **IfSAR PRESENT OPERATING STATUS**

DEM generation from the IfSAR mapping technique is offered by a small number of commercial companies in comparison to the plethora of aerial photography and lidar companies available today. Commercial companies offer DEM users with options to purchase data from an archive (e.g. Intermap airborne IfSAR and Airbus spaceborne world DEM) as well as offer project specific data collections (e.g., Furgo or Intermap). Commercially available IfSAR providers are listed Tables 7.3 and 7.4

Many commercial companies now have software that allows users themselves to generate products from raw data. The quality of these products depends on the type of data collection (single or repeat-pass), the number of interferometric pairs available over the region of interest, the amount of decorrelation and atmospheric distortion, baseline length for the interferometric pairs, and the wavelength of the operating sensor(s). The principal companies marketing these technologies and products are **Intermap**, **Furgo**, **Bradar**, **Airbus**,

e-Geos, and, MDA. In addition to commercial companies that market software there are several freeware packages (e.g. ROIPAC or ISCE) that can be used to generate DEMs from spaceborne IfSAR data for non-commercial purposes. The most accurate and reliable sources of IfSAR DEM data are generated using single-pass systems.

**Table 7.3 Summary of the key parameters of airborne IfSAR systems. Table abbreviations: wavelength ( $\lambda$ ); polarization (POL); ground sample distance (GSD); elevation vertical accuracy (RMSE); IfSAR Pass is IP; Single is S; Repeat is R, data collection type project (P) and archived (A).**

Sensor	Country	$\lambda$	POL	DEM	GSD	RMSE	IP	Data
STAR	Canada	X	HH	DSM/ DTM	5 m	0.5-6 m	S	P/A
GeoSAR	USA	X	VV	DSM/ DTM	3-5 m	0.5-5 m	S	P
	USA	P	HH/VV	DSM/ DTM	5 m	2 - 6 m	S	P
BRADAR	Brazil	X	Quad	DSM	5 m	10 m	S	P
	Brazil	P	Quad	DSM	5 m	10 m	S	P
Glisten	USA	Ka	HH	DSM	3 m	0.15-2 m	S	P

**Table 7.4 Summary of the key parameters of select spaceborne SAR systems suitable for deriving elevation data via IfSAR methods. Table abbreviations: wavelength ( $\lambda$ ); polarization (POL); ground sample distance (GSD); elevation vertical accuracy (RMSE); IfSAR Pass is IP; Single is S; Repeat is R, data collection type project (P) and archived (A).**

Sensor	Country	$\lambda$	POL	DEM	GSD	RMSE	IP	Data
Tandem-X	Germany	X	Quad	DSM/DTM	12 m	10 m	R	P/A
COSMO-SkyMed	Italy	X	Quad	DSM	5 - 30 m	10 m	R	P
SRTM	USA	C	VV	DSM	30 - 90 m	8 m	S	A

## Airborne IfSAR Systems

### STAR – Intermap Technologies Inc.

Intermap is a long-time provider of airborne radar mapping products. The foundation of the company’s success lies in its innovations in 3D digital modeling, geometric imaging, data acquisition, and data aggregation. Today, Intermap is a global geospatial solutions leader focused on improving the ways people, businesses, and governments use location-based information. Intermap does this through its products and services, which include the NEXtMap® five-meter elevation datasets, NEXtMap World 30™, AdPro®, LinkPro®, RiskPro™, Geospatial Services, and Data Fusion. Foundational to these products and services is the NEXtMap 3D digital models, created using IfSAR technology and integrated third-party data.

Intermap’s IfSAR systems (Figure 7.22. STAR-3 and STAR-6) configuration consists of a synthetic aperture radar sensor with two X-band radar antennas, a global positioning system (GPS) and inertial navigation system (INS) components. The radar pulse signals are collected from two radar antennas and compressed by digital match filtering to extract the interferometric phase information that is then processed to derive elevation data and radar imagery. The GPS/INS system provides highly accurate position and orientation information without the need for in-scene ground control. Positioning technologies, such as GPS and INS coupled with differential GPS (DGPS) post processing software have reduced ground control survey costs, while simultaneously reducing the

need for ground control surveys by making direct sensor orientation possible. Combining the SAR interferometric information and the GPS/INS navigation results allow for the creation of a highly accurate ortho-rectified radar image and digital elevation model, without the need for the deployment of in-scene ground control. Table 7.5 lists the system parameters of the STAR-3/6 radars.

Antennas are mounted to a solid invar frame with a ~1 m physical separation that provides a temperature and mechanically stable **interferometric baseline**. The frame is attached to the bottom of the aircraft on an azimuth steerable pedestal thus allowing for mapping on either side of the aircraft. Motion measurement data is obtained using a combination of DGPS data collected using an Ashtech Z-12 receiver and a Honeywell 770 IRU. The IMU is mounted to the same invar frame as the radar antennae to minimize lever arm errors between the IMU and antenna phase centers.



**Figure 7.22. The STAR-3 (left image) and STAR-6 (right image) radars are flown on a Learjet 36 with the antennas mounted to an invar frame contained in the large dome on the underside of the aircraft. (Figures courtesy of Intermap Technologies Inc.)**

Flight plans are generated using a customized flight planning tool and uploaded to the radar prior to flight. The radar operates in the Ping-Pong mode with the interferometric channels sharing a single receiver. Radar signal data and motion data are recorded directly to an onboard disc system. Data are processed on an array of 3D workstations, quality control checked prior to mosaic and post processing into final products delivered to the customer. Post processing steps include interferometric processing using proprietary software that included averaging of multiple IfSAR flight lines (from overlapping flight lines and tie lines) where possible, and filtering of the interferogram to reduce phase noise using a Gaussian filter. Reference ground elevation points are used as seed points to assist with phase unwrapping, to provide elevations that link ground elevations to the interferogram. This process creates IfSAR data that requires merging and editing to produce the final NEXTMap DSM and DTM products with a 5m ground sampling distance (GSD) in grid format using horizontal datum NAD83, the latest geoid model, and georeferenced to latitude and longitude in decimal degrees and seconds. Table 7.5 provides a summary of the main system parameters.

**Table 7.5. STAR-3 and -6 System Parameters**

Parameter	STAR-3	STAR-6
Peak Transmit Power	8 kW	8 kW
Bandwidth	67/135 MHz	67.5/135 MHz
Center Frequency	9.55 MHz	9.55 GHz
Baseline Length	0.92 m	1 m
Baseline Tilt Angle	0°	0°

Platform Altitude	10,000 m	10,000 m
-------------------	----------	----------

The DEM data editing is employed to produce the commercial **NEXTMap** products. Editing included the following steps. All voids in the data were populated with tie line and/or overlapping flight-line data where possible, and recalculated using ancillary elevation data (data are tied and warped to the DSM bare ground), or interpolated where no ancillary data were available. All water bodies were smoothed to the elevation of the surrounding shoreline. For example, lakes of 400 m or more in length were flattened and set to a constant elevation. Single line streams up to 20 m in width were delineated using 3D vectors, whereas double line streams greater than 20 m wide were collected as 3D polygons. Both types of streams were stepped down in height to match the surrounding water levels to maintain monotonicity (e.g. water flowing downstream). DSM and DTM examples are provided in Figure 7.23.

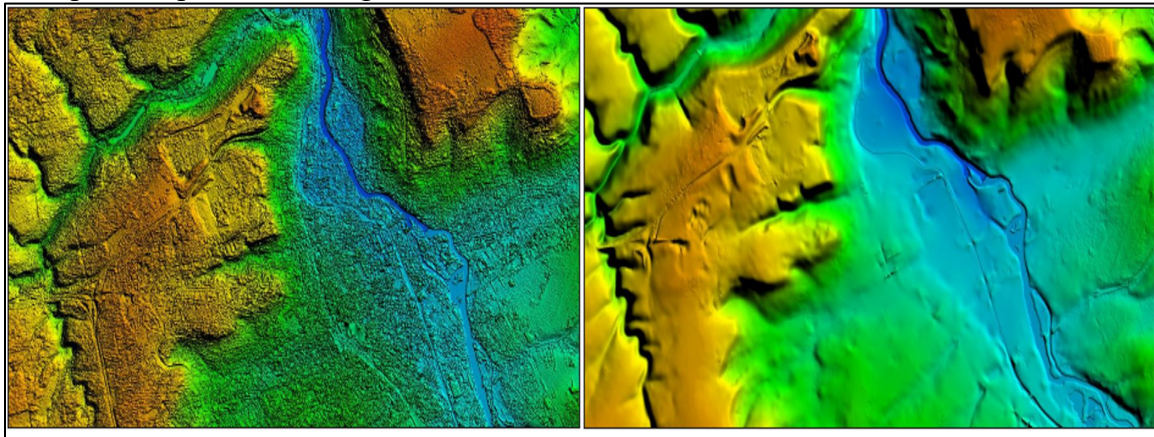


**Figure 7.23.** An example of the NEXTMap DEM products: Left - DSM depicting elevations of buildings and vegetation; right - DTM of the same area. The DTM in barren areas had been “smoothed” using proprietary 3D editing tools to remove noise (up to 30 cm) in the DSM data (Figure courtesy of Intermap Technologies Inc.).

Additional processing was applied to create the DTM where elevations of features such as vegetation and buildings were removed, based on a set of edit rules described in the Intermap Handbook (Intermap, 2011). Intermap offers a variety of IfSAR derived DEMs and SAR image products around the globe, under the NEXTMap product name. The NEXTMap products vary in accuracy and specification worldwide as outlined in Table 7.6.

**Table 7.6. STAR-Derived **NEXTMap** Mapping Products Specifications**

DATA TYPE	NORTH AMERICA			PUERTO RICO, JAMAICA, CENTRAL / SOUTH AMERICA		
	RESOLUTION	ACCURACY	COVERAGE AREA*	RESOLUTION	ACCURACY	COVERAGE AREA*
DSM, DTM	5m	< 1m LE90% (vertical)	40%	5m	< 3m LE90% (vertical)	40%
		1–3m LE90% (vertical)	40%		3–5m LE90% (vertical)	40%
		> 3m LE90% (vertical)	20%		> 5m LE90% (vertical)	20%
ORI	.625m	3m CE90% (horizontal)	4%	—	—	—
	1.25m	4m CE90% (horizontal)	94%	1.25m	4m CE90% (horizontal)	90%
	2.50m	5m CE90% (horizontal)	2%	2.50m	5m CE90% (horizontal)	10%

DATA TYPE	WESTERN EUROPE			DEMOCRATIC REPUBLIC OF THE CONGO		
	RESOLUTION	ACCURACY	COVERAGE AREA*	RESOLUTION	ACCURACY	COVERAGE AREA*
DSM, DTM	5m	< 1m LE90% (vertical)	40%	5m	< 3m LE90% (vertical)	40%
		1–3m LE90% (vertical)	40%		3–5m LE90% (vertical)	40%
		> 3m LE90% (vertical)	20%		> 5m LE90% (vertical)	20%
ORI	.625m	3m CE90% (horizontal)	4%	—	—	—
	1.25m	4m CE90% (horizontal)	94%	1.25m	4m CE90% (horizontal)	90%
	2.50m	5m CE90% (horizontal)	2%	2.50m	5m CE90% (horizontal)	10%

DATA TYPE	MALAYSIA, AND PARTS OF INDONESIA AND AUSTRALIA			PHILIPPINES, SOLOMON ISLANDS, VANUATU, AND PARTS OF INDONESIA		
	RESOLUTION	ACCURACY	COVERAGE AREA*	RESOLUTION	ACCURACY	COVERAGE AREA*
DSM, DTM	5m	< 1m LE90% (vertical)	40%	5m	< 3m LE90% (vertical)	40%
		1–3m LE90% (vertical)	40%		3–5m LE90% (vertical)	40%
		> 3m LE90% (vertical)	20%		> 5m LE90% (vertical)	20%
ORI	.625m	3m CE90% (horizontal)	4%	—	—	—
	1.25m	4m CE90% (horizontal)	94%	1.25m	4m CE90% (horizontal)	90%
	2.50m	5m CE90% (horizontal)	2%	2.50m	5m CE90% (horizontal)	10%

### **GeoSAR – Fugro EarthData Inc.**

Fugro EarthData is a global remote sensing, mapping, and GIS services organization that provides customized products and solutions to support a wide range of land-use and natural resource management activities. GeoSAR, their primary radar remote sensing mapping system, came about from a program initiated to develop a dual frequency airborne radar interferometric mapping instrument designed to meet the mapping needs of a variety of users in government and private industry. Program participants consisted of the **Jet Propulsion Laboratory (JPL)**, EarthData International (previously Calgis, Inc.), and the California Department of Conservation with funding provided initially by DARPA and subsequently by the **National Geospatial-Intelligence Agency (NGA)**. The program was begun to address the critical mapping needs of the California Department of Conservation to map seismic and landslide hazards throughout the state. GeoSAR operates X-band and P-band radars designed to measure the terrain elevation at the top and bottom of the vegetation canopy. The GeoSAR radar flies onboard a Gulfstream-II aircraft and is a dual-frequency (P- and X-band) interferometric Synthetic Aperture Radar (SAR), with HH and HV (or VV and VH or full quad) polarization at P-band and VV polarization at **X-band** [Hensley et al, 2001] that collects data on both sides of the aircraft simultaneously. The radar hardware onboard the Gulfstream-II aircraft is supplemented with a **Laser-Baseline Measurement System (LBMS)** which provides real-time measurements of the antenna baselines in a platform based coordinate system that is tied to the onboard **Embedded GPS Inertial (EGI)** units. The onboard data collection via the Automatic Radar Controller also records navigation data from the aircraft’s GPS/INU system, the laser-based antenna-baseline measurement system, and raw signal data from X- and P-band radars.

The **P-band** antenna system is mounted in the port and starboard wingtip pods providing a long antenna-baseline of about 20 meters. **X-band** antennas are mounted in pairs under the wings with an antenna-baseline of 2.5 meters. The system can collect data in continuous strips greater than 500 km in length. Also, upgraded at the same time were the analog-to-digital converters to provide higher fidelity radiometric and height mapping

products. GeoSAR maps a 20-km swath by collecting two 10-km swaths on the right and left sides of the plane as shown in Figure 7.24.

Radar operations are controlled by a command disk generated preflight by the Mission Planning Software. Real-time data collection is controlled in-flight via an **Automatic Radar Controller (ARC)** that sets data collection windows, performs Built-In Tests (BIT's) before and after each data take, and automatically turns the radar on and off during data acquisition. Raw radar data is recorded on high-density digital tape recorders for subsequent, post-flight processing. The processor incorporates several algorithms used to remove radio frequency interference (RFI) at **P-band**, focus the P-band data with its large synthetic aperture, and for regridding and mosaicking the data. The expected map accuracy of the **X-band** system is sub-meter in bare surface regions and 1-4 m in vegetated areas through a combination of X-band and P-band data. The system has undergone several upgrades since it began operational service. First the system incorporated a smaller and more accurate second generation LBMS to track the interferometric baselines, greatly increasing the mapping swath at X-band. Secondly, the system was augmented with a lidar mapping system that collects nadir pointing elevation data with 15-20 cm mapping accuracy. Lidar data are used to provide very accurate control for large area topographic mapping projects. Upgrades to the digital system replaced the high-speed tape based storage system with new disk based storage devices, thereby increasing the amount of data that could be collected in a single flight line. Table 7.7 provides a summary of the main system parameters.

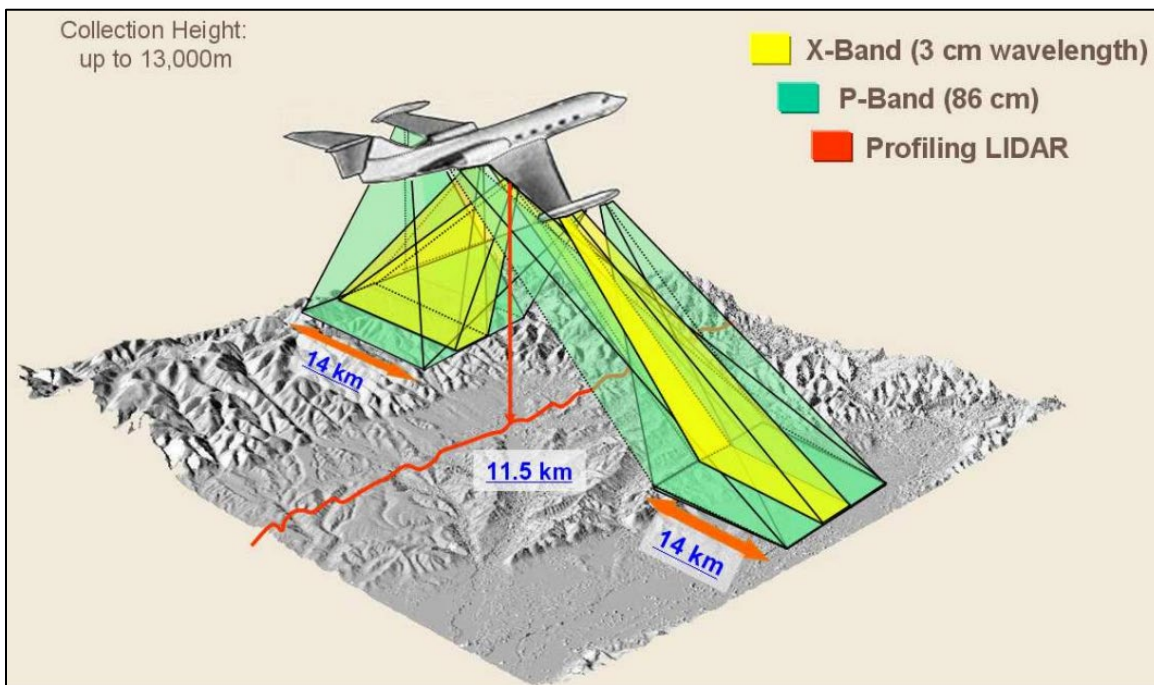


Figure 7.24. The GeoSAR radar flies aboard a Gulfstream-II modified jet at high altitude and high-speed. This configuration makes it efficient for wide-area mapping applications, acquiring data on both sides of the plane simultaneously in **X-band** and **P-band** at a rate of approximately 300 km<sup>2</sup> per minute, per band (~400 MB per second).

Table 7.7. **GeoSAR System Parameters**

Parameter	<b>P-Band</b> Value	<b>X-Band</b> Value
Peak Transmit Power	4 kW	8 kW

Bandwidth	80/160 MHz	80/160 MHz
Center Frequency	350 MHz	9.755 GHz
Baseline Length	20 m and 40 m	2.6 m or 5.2 m
Baseline Tilt Angle	0°	0°
Platform Altitude	5,000 m to 13,000 m	5,000 m to 13,000 m

Figure 7.25 provides an example of the DEMs generated using the X-band and P-band IfSAR over Monarch Grove, CA. The eucalyptus tree stand highlighted in the imagery shows up extremely well at X-band but is nearly undetectable in the P-band data because of the increased penetration into the canopy.

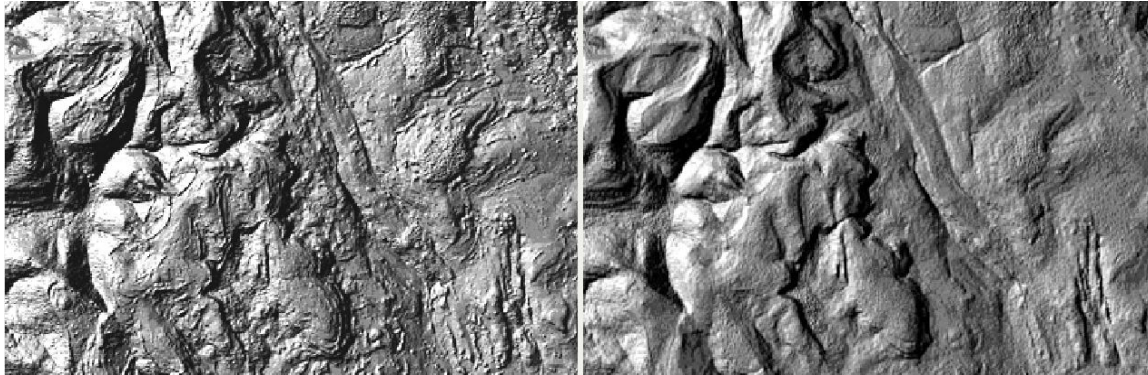


Figure 7.25. GeoSAR **X-band** DSM (left) and **P-band** (right) DEM data.

## BRADAR

**Bradar Industrial S.A.** is a technology based company, specialized in remote sensing and radar aerial and ground surveillance. Bradar is engaged in the development, construction, service, and sale of radars and other sensors for use in defense, and security and surveillance sectors. It also offers remote sensing solutions for mapping and monitoring the earth surface. The company was founded in 1984 and is based in São José dos Campos, Brazil. Bradar Industrial S.A. operates as a subsidiary of Embraer S.A. The OrbiSAR-1 was designed for this purpose. This system generates high-precision altimetry and planimetric maps through the X and P radar bands. Table 7.8 gives a summary of the main system parameters.

Table 7.8. BRADAR System Parameters

Parameter	<b>P-Band</b> Value	<b>X-Band</b> Value
Peak Transmit Power	4 kW	8 kW
Bandwidth	80/160 MHz	80/160 MHz
Center Frequency	350 MHz	9.755 GHz
Baseline Length	20 m and 40 m	2.6 m or 5.2 m
Baseline Tilt Angle	0°	0°
Platform Altitude	5,000 m to 10,000 m	5,000 m to 10,000 m

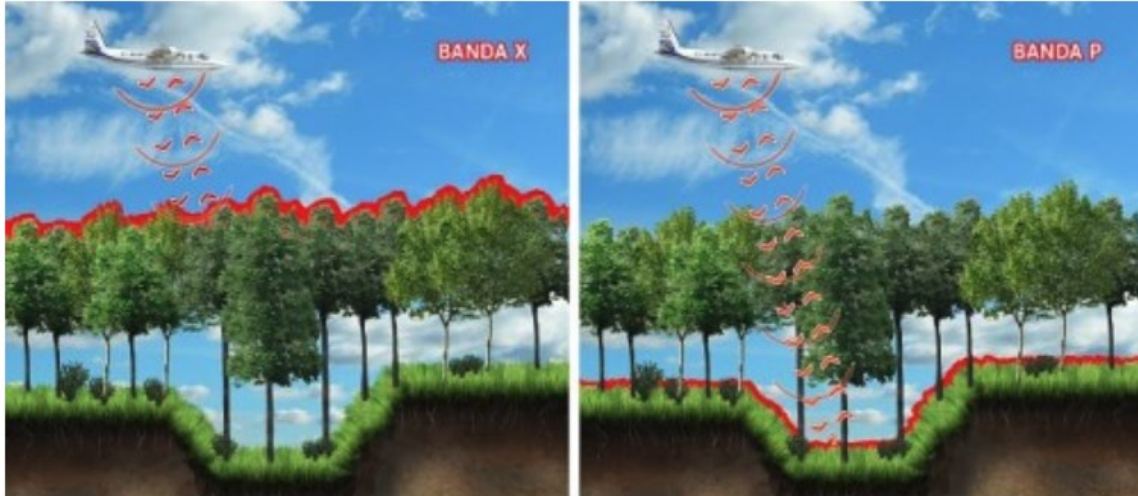


Figure 7.26 illustrates the X and P bands signals. The **X-band** waves are reflected and scattered through the treetops, while the **P-band** penetrate the foliage and is reflected by the ground and the dense trunks, allowing the soil mapping under the vegetation.

### **GLISTIN** Ka-Band Ice Topography Mapper

As interferometric mapping technology evolves, systems are emerging to meet specific operational or scientific needs. An example of this is the development of the Ka-band (8 mm wavelength) airborne Glacier and Land Ice Surface Topography Interferometer (GLISTIN) mapping radar developed by NASA/JPL as part of the International Polar Year (IPY) to map glacier and ice topography [Moller, et al., 2011, Hensley, 2016].

The GLISTIN instrument was developed as an adaptation of the NASA/JPL UAVSAR L-band radar that was designed for repeat pass radar observations of deforming surfaces [Hensley et al., 2008]. This radar is flown in a pod mounted underneath the fuselage of a Gulfstream III aircraft as shown in Figure 7.27. The lower insert shows the mounting of Ka-band antenna that have a baseline length of 25 cm and are oriented 45° from the horizontal. Because the along track dimension of the antennas is 50 cm detailed along track SAR imagery of about 30 cm is generated. The cross-track ground resolution (GSD) of the SAR is 3 m. Ka-band was chosen to minimize the amount of penetration into snow and ice. Measurements of interferometric penetration into dry snow, i.e., the amount the interferometric elevation measurements were below the air/snow interface, were made at Summit Camp in Greenland and found to be on the order of 25 cm [Hensley, et al 2016].



**Figure 7.27. The NASA Gulfstream III with pod configured for Ka-band interferometry. Lower insert shows close-up with details of the IfSAR antennae.**

This system was designed to observe ice topographic measurements. For ice topography applications measurements with 100 m spatial resolution are needed and thus spatial averaging to this resolution allows the system to meet its 15-20 cm height precision requirement. A **Ka IfSAR** derived DEM collected on a May 1, 2009 near the Greenland coast having about 800 m of topographic height variation is presented in Figure 7.28, along with the corresponding IfSAR correlation and IfSAR DEM height precision map derived from the correlation data. Elevation precision decreases across the stripmap mode swath (from left, near range {NR} to right, far range {FR}) due to lower signal to noise. This reduction in elevation precision from NR to FR is typical of IfSAR mapping systems. Operational IfSAR mapping systems collect multiple overlapping flight lines of data to minimize the across-track height error. For example, a final DEM maintains a 10 cm RMSE elevation accuracy almost everywhere in the output DEM.

Change in ice sheet topography is an important metric in quantifying and understanding the impacts of climate change. Most measurement of ice sheets to monitor topographic change has used either spaceborne or airborne lidar systems. Satellite radar altimetry is most accurate over flat areas, but performs poorly over the steep coastal regions where substantial amounts of change are located. Airborne laser altimetry is better suited to these steep regions but is limited in spatial coverage and swath width (500m), thus making it impractical for use at the continental scale over Antarctica. **GLISTIN** was designed to provide a wide swath ice topography measurement with high precision to augment lidar ice topography measurements. Key to the design of the GLISTIN instrument was the desire for the radar signal to have minimal penetration into the ice so that measurements could be easily cross compared with lidar measurements. This was

accomplished using a very high frequency of 35 GHz (0.008 m wavelength) SAR. Table 7.9 gives a summary of the main system parameters.

**Table 7.9. GLISTIN System Parameters**

Parameter	Values
Peak Transmit Power	75 W
Bandwidth	80 MHz
Center Frequency	35.66 GHz
Baseline Length	0.0084 m
Baseline Tilt Angle	45°
Platform Altitude	8,000 m to 12,000 m
Boresight Look Angle	35°
Polarization	Horizontal

A **Ka IfSAR** derived DEM collected on a May 1, 2009 near the Greenland coast having about 800 m of topographic height variation is presented in Figure 7.28, along with the corresponding IfSAR correlation and IfSAR DEM height precision map derived from the correlation data. Reduction in elevation precision from NR to FR is depicted in Figure 7.28. This phenomenon is typical of IfSAR mapping systems and mitigated by collecting multiple overlapping flight lines so that final DEM products maintain a consistent RMSE elevation accuracy almost everywhere in the output DEM.

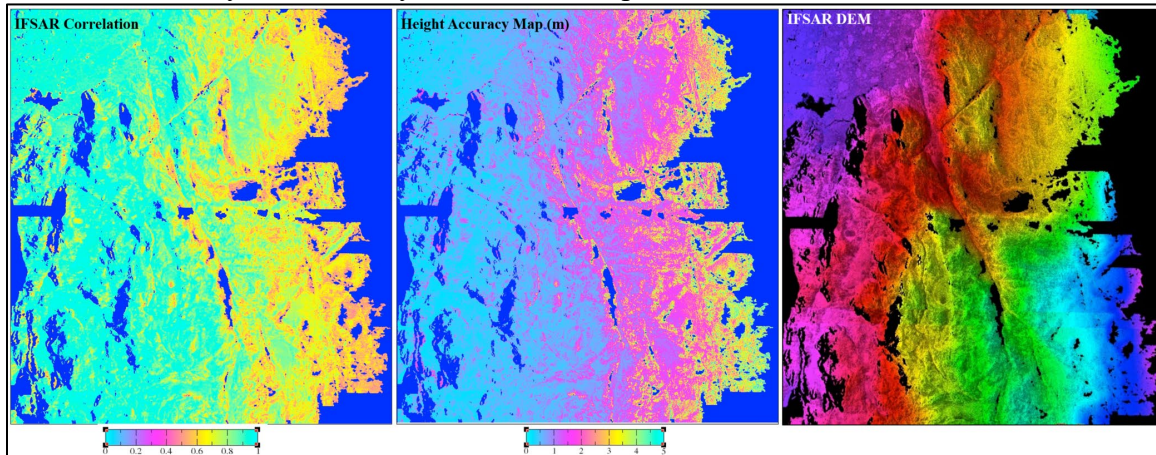


**Figure 7.28. Interferometric correlation data (left image), IfSAR derived height error map (middle image) generated from the correlation data. Note the height accuracy varies from 30 cm in the NR (left handed side of the middle image, light blue in color) to about 3 m in the FR (right handed side of the middle image, yellow in color). The far-right image is the **Ka-band IfSAR** derived DEM where the elevations are color coded with a wrap of 800 m (from pink to red to green to pink again) to represent an elevation change of 800 m.**

### **Spaceborne IfSAR Systems**

#### **TanDEM-X Sensor – Airbus**

TanDEM-X (‘TerraSAR-X add-on for Digital Elevation Measurement’) is a SAR Earth observation satellite system that consists of a pair of almost identical TerraSAR-X radar satellites that form a high-precision IfSAR system. It marks the first bistatic IfSAR

mission, formed by adding a second, almost identical spacecraft, to TerraSAR-X and flying the two satellites in a closely controlled formation with typical distances between 250 and 500 m. Primary mission objective is the generation of a consistent global digital elevation model with an unprecedented accuracy. This system generated the **WorldDEM** product which was made possible because of a public private partnership between Airbus and the **German Aerospace Centre (DLR)**. The approximately 150 million square kilometers of land surface were scanned from space by the TanDEM-X IfSAR mission. The global coverage achieved by TanDEM-X is also unparalleled – all land surfaces were scanned multiple times and the data was then processed to create elevation models. The WorldDEM accuracy surpasses that of any global satellite-based elevation models available today and defines a new industry standard. The WorldDEM is a complete pole-to-pole coverage DEM with unrivalled horizontal and vertical accuracy and quality. An example of the WorldDEM is presented in Figure 7.29. Table 7.10 gives a summary of the main system parameters.

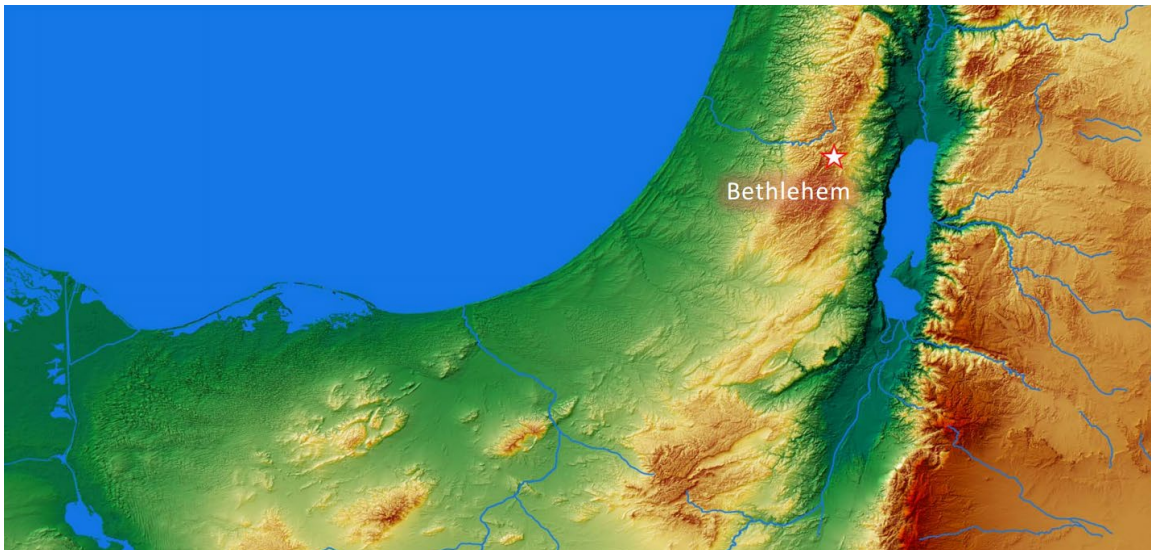


Figure 7.29. Bethlehem **WorldDEM** example, completed December 23, 2016.

Table 7.10. **Tandem-X** System Parameters

Parameter	Values
Peak Transmit Power	10-15 W
Bandwidth	100 MHz
Center Frequency	9.65 GHz
Baseline Length	200-500 m
Platform Altitude	513 km
Incidence Angle Range	20°-55°
Polarization	Horizontal

Airbus holds the exclusive commercial marketing rights for the data and refines the elevation models per the needs of commercial users worldwide. Airbus provides an

expanded IfSAR derived product portfolio based on the **WorldDEM** data, including DEM, DTM, Global Ocean Shoreline, Waterbody Map, and Global Airport / Harbor Map.

### **COSMO-Sky-Med – e-Geos**

COSMO (Constellation of small Satellites for Mediterranean basin Observation) SkyMed is a constellation of SAR satellites that can be utilized in RPI. COSMO SkyMed was commissioned and funded by the **Italian Space Agency (ASI)** and the Italian Ministry of Defense (MoD) as an end-to-end earth observation system civilian and defense system. The SAR constellation is comprised of four low earth orbit mid-sized satellites each equipped with multi-mode high resolution X-band SARs (Figure 7.30). Table 7.11 gives a summary of the main system parameters.

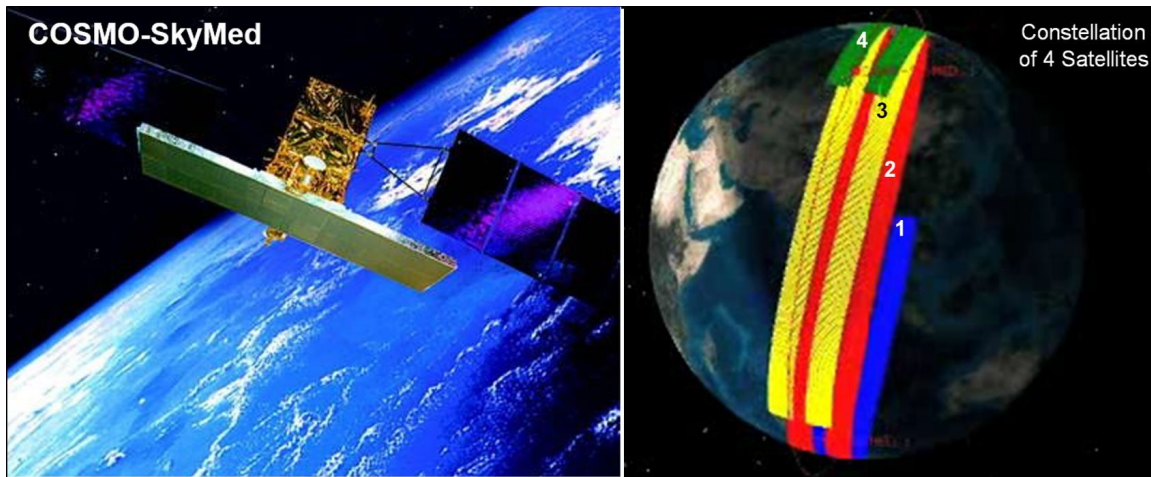


Figure 7.30. **COSMO-SkyMed** X-band constellation

Table 7.11. **COSMO-Sky-Med System Parameters**

Parameter	Values
Peak Transmit Power	17 W
Bandwidth	400 MHz
Center Frequency	9.6 GHz
Baseline Length	151 km
Platform Altitude	619 km
Incidence Angle Range	25°-50°
Polarization	Horizontal

**e-GEOS** is the worldwide exclusive data distributor for COSMO-SkyMed data and products. e-GEOS, an ASI (20%) / Telespazio (80%) company, is a leading international player in the earth observation and geospatial information business. e-GEOS offers a unique portfolio of application services thanks to the superior monitoring capabilities of the COSMO-SkyMed constellation and provides environmental monitoring, rush mapping in support to natural disaster management, specialized products for defense and intelligence, maritime surveillance, interferometric products for landslide and ground subsidence analysis, and thematic mapping for agriculture and forestry. e-GEOS operates

the Matera Space Centre for acquisition, archiving and processing of multi-mission satellite data.

The DEM products are derived by mean interferometric processing of the SAR Level 1A co-registered products, in any acquisition mode except polarimetric in an automatic way. The DEM products consist of the ellipsoidal height map and the associated height error map. The attributes defining the DEM products are derived from the SAR image couple, with some substantial changes (e.g. due to the change of the image projection). The DEM product is presented in UTM cartographic coordinate system with respect to the WGS84 ellipsoid, different from the input geometry (slant-range). In the case of a DEM product originated from ScanSAR interferometric couple, output is presented in a single layer having elementary beams mosaicked in the range direction. The same constraints already shown for interferometric product also exist in the generation of the DEM products. The DEM and error map are represented in the same geometry with the same pixel spacing and have the same size. The accuracies are strongly dependent on the coherence value and the geometric configuration of the acquisition and scene, as well as the quality of the input ground control points used during the geometric calibration. There are a four IfSAR products for the end user to select from to create a DEM using COTS software. They are called L1A, L1B, L1C, and L1D. Each product type has a distinct set of processing applied to them.

The L1A product processing is aimed at generating **Single-look Complex Slant (SCS)** products. The SCS product, obtained after the L1A processing, contains focused data in complex format, in slant range and zero Doppler projection. Gain receiver compensation, internal calibration, data focusing, statistics estimation of the output data and data formatting into output are applied to this product.

The L1B product processing is aimed at generating **Multilook Detected Ground (MDG)** products, starting from input (L1A) data. An MDG product, obtained after L1B processing, contains focused data, detected, radiometrically equalized and in ground range/azimuth projection, and multi-looking for speckle reduction. Image detection (amplitude), ellipsoid ground projection, statistics evaluation, and data formatting are applied to this product.

The L1C product processing is aimed at generating **Geocoded Ellipsoid Corrected (GEC)** products. A GEC product, obtained after L1C processing, contains focused data, detected geo-located on the reference ellipsoid and represented in a uniform pre-selected cartographic presentation.

The L1D processing is aimed at generating Geocoded Terrain Corrected (GTC) products. A GTC product, obtained after L1D processing, contains focused data projected onto a reference elevation surface in a regular grid obtained from a cartographic reference system. The processing performed on L1B input data is GEC processing with the use of the DEM for map projection.

### **SRTM – NASA-NGA**

The Shuttle Radar Topography Mission (SRTM) C-HH IfSAR sensor was flown on board the Space Shuttle Endeavour during mission STS-99. It was a single IfSAR mission that operated from February 11-22, 2000, making it the world's first IfSAR to acquire spatially-continuous elevation information over 80% of the Earth's land mass [Farr et al., 2007]. SRTM utilized two SAR antennae with a fixed-baseline of 60 m at an altitude of 233 km

and an orbit inclination angle of 57°, collecting data between 60° N and 57° S latitude [Farr et al., 2000]. The C-band antennas were operated in a two-beam ScanSAR mode such that four narrow but overlapping sub-swaths were generated sequentially with incidence angles ranging between 30° and 60° [Farr et al., 2000]. Of the Earth’s land mass covered by SRTM, 99.97% was mapped with at least one Shuttle overpass, 94.59% with at least two passes, 49.25% with at least three passes, and 24.10% with at least four passes.

The C-band IfSAR data were interferometrically processed by the Jet Propulsion Laboratory (JPL, Pasadena CA) and made available to the public via the National Map Seamless Data Distribution System administered by the USGS (<http://seamless.usgs.gov>). The interferometric processing included averaging of multiple data acquisitions where possible, and filtering of the interferogram to reduce phase noise and improve the phase unwrapping process [Hensley et al., 2000; Smith and Sandwell, 2003, Rodriguez,].

NASADEM is a modernization of Shuttle Radar Topography Mission elevation data designed to improve DEM quality and provide additional data layers. The project is reprocessing raw radar signal data using improved unwrapping algorithms and mosaicking the strip data using spaceborne lidar data from ICESat data for improved ground control that was unavailable at time of original processing. The most significant improvements involve void reduction through the improved phase unwrapping and using ICESat data for control. The allowed NASADEM to make a so-called height ripple error correction that reduced elevation artifacts in the strip elevation data resulting from under sampled motion metrology of the antenna boom. Remaining voids are primarily filled with PRISM and ASTER DEM data. A new post-processing module creates DEM-derived layers from void-filled and merged elevation data. New output layers include imagery, height precision, incidence angle, slope and curvature and vegetation layers. Data will be released to the LPDAAC in 2017. Table 7.12 gives a summary of the main system parameters.

**Table 7.12. SRTM System Parameters**

Parameter	Values
Peak Transmit Power	1.7 W
Bandwidth	160 MHz
Center Frequency	5.3 GHz
Baseline Length	60 km
Platform Altitude	233 km
Incidence Angle Range	57°
Polarization	Horizontal

Similar DSM finishing techniques performed on the X-HH IfSAR data provided by Intermap were performed on the SRTM data. The SRTM data were segmented into 1-degree cells (equivalent to 64 of the Intermap 7.5’ tiles) comprised of elevations generated by averaging all data from the multiple passes that fell within that cell. The National Geospatial-Intelligence Agency (NGA) performed the quality assurance checks and carried out several additional editing steps [Slater et al., 2006]. First, spikes and wells were removed if they exceeded 100 m compared to surrounding elevations. Second, small voids (16 contiguous posts or less) were filled by interpolation of surrounding elevations. Large voids were left in the data. Third, the ocean elevation was set to 0 m, lakes of 600 m or

more in length were flattened and set to a constant height, rivers over 183 m wide were delineated and monotonically stepped down in height, and islands were depicted if they had a major axis exceeding 300 m or their relief was greater than 15 m. The C-band DSM has a 30 m and 90 m ground sample distance (GSD) both with specifications of 16 m absolute vertical height accuracy, a 10m relative vertical height accuracy (at a local scale of ca. 200 km), and 20 m absolute horizontal accuracy, all at the 90% confidence level [Rabus et al., 2003].

## COMPARISON WITH OTHER TECHNOLOGIES

Commercially available IfSAR systems can acquire data in the absence of the sun (day or night operation), in most weather and atmospheric conditions, through clouds, at high collection rates and over large and remote geographic areas. These characteristics make these systems a viable alternative to conventional aerial photography and lidar technologies for large area topographic and land cover mapping.

Each type of sensor is sensitive to different aspects of the surface under observation and therefore measures height differently depending on surface type and ground cover. All the above sensors make height measurements that depart from an “idealized height sensor” that gives the height measurement at precisely one point. Only for simple surfaces or after appropriate post processing of the data can the height measurements of the three types of sensors be directly compared with point measurements like those obtained by DGPS surveys.

The desired elevation measurement is application dependent. Flood plain applications require DEMs to have all vegetation and buildings removed, and water constriction features such as bridges, fences and power poles edited from the data. However, for flight obstruction or forest mapping it is desired to leave some or all the elevations unaltered. Each of the different sensor technologies has strengths and weaknesses depending on the desired height measurement for an application. In fact, a synergistic combination of measurements from two or more of the above sensors can produce the best possible product.

As the variety of IfSAR, lidar, and photogrammetric sensors is quite numerous, and performance parameters continuously improving for all three types of sensors, only very general comparisons of the sensor characteristics are presented.

IfSAR systems can acquire data in the absence of the sun (day or night operation), in most weather and atmospheric conditions, through clouds, and at high collection rates. These characteristics make these systems a viable alternative to conventional aerial photography and lidar technologies for large area topographic and land cover mapping.

### **Photogrammetry**

Fully explained in Chapter 6, photogrammetric sensors, like IfSAR systems, generate both imagery and height data and have been operated on both airborne and spaceborne platforms. Unlike aerial or spaceborne photogrammetry, IfSAR missions can be flown without regard to sun angle. Flights may take place at night or in conditions of inclement weather provided the conditions are such that the image formation process is not degraded. Airborne optical cameras continue to generate extremely fine resolution (often sub-meter) imagery without the troublesome layover and shadow problems of radar. However, radar interferometers are proving to be a cost-effective method for wide area, rapid mapping

applications, and do not require extensive hand-editing and tie pointing. Additionally, because IfSAR systems often fly at greater altitudes, they can operate in congested air-traffic corridors that are often difficult to image photogrammetrically. Mapping in tropical regions that are often cloud-covered can be done more reliably with IfSAR systems that penetrate clouds. Urban mapping is a challenging venue for mapping by IfSAR systems due to the extremely complex scattering environment. Although some high-resolution systems have shown promise for urban mapping, photogrammetry still has inherent advantages for this application.

Densely vegetated surfaces can be problematic for both sensors if bare surface elevations are desired. Photogrammetric true ground surface heights can only be obtained if sufficiently large gaps are present in the canopy. These points, usually determined manually, are then extrapolated to other portions of the canopied area to produce bare earth height maps. Heights measured by IfSAR systems are reflective surface heights and can lie anywhere within the canopy. Longer wavelength systems penetrate deeper into the canopy but the exact location within the canopy corresponding to the height measurement is not easily determined. IfSAR correlation has information about the vertical structure of the canopy and has the potential of providing corrections to measure bare surface elevations [Hokeman and Varekamp, 2001].

Unlike photogrammetric and lidar systems, IfSAR systems can generate height error maps on a pixel-by-pixel basis [Hensley and Webb, 1994]. These images provide an estimated relative statistical height error as described earlier. These products are extremely useful for ascertaining whether an IfSAR derived DEM is suitable for a mapping application and for locating problematic regions within the DEM.

### **Lidar**

Airborne topographic lidar is fully explained in Chapter 8. Lidar like IfSAR is an active sensor providing its own illumination and similarly records the time delay between transmit and receipt of reflected signals from the surface. Employing a very narrow beam so that the projected footprint on the ground is typically 75 meters or less from space (several feet from airborne sensors), lidar systems obtain one or more height measurements per pulse. The number of height measurements is dependent upon the vertical structure of objects within the beam and the type of lidar system. Some lidar systems are equipped to only record a single time delay per pulse whereas most lidar systems record time delays for multiple samples exceeding a signal level threshold. By scanning cross track to either side of the nadir point of the aircraft and rapidly pulsing the laser, reasonable mapping swaths are obtained. Operating at optical instead of microwave frequencies, lidar systems do not penetrate clouds and other atmospheric obscurants.

Unlike IfSAR systems lidars are not imaging sensors, though they do provide intensity returns or reflectance images. Applications, where contextual information that is not easily derived from height data alone, favor IfSAR and photogrammetric mapping sensors. Classification studies and resource inventory surveys are examples where imagery plays a vital role in separating and identifying vegetation and crop types, geologic structures, and various anthropogenic uses. Water body mapping and delineation is often possible with IfSAR systems depending on the frequency of operation and the roughness of the water body surface, whereas topographic lidar systems do not obtain good height

measurements over water. Chapter 10 explains the advantages of bathymetric and topobathymetric lidar sensors for mapping water elevations and submerged topography.

Lidar systems have become the sensor of choice for mapping vegetated regions when elevation measurements beneath the canopy are needed. True ground surface elevation measurements are obtained after a post processing step to insure the reflective surface does not arise from within the vegetation canopy. As previously noted, heights measured by IfSAR systems are reflective surface heights and can lie anywhere within the canopy, but with proper frequency selection and use of correlation data has the potential of providing corrections to measure bare surface elevations. Larger swaths possible with IfSAR mapping systems can substantially reduce the time to collect data over large areas.

## **USER APPLICATIONS**

Fine resolution topographic measurements have applications throughout the commercial, civilian, and military sectors. Applications include, for example, land slope stability and land-slide characterization, land-use classification and change monitoring for agricultural and military purposes, flood plain and hydrologic modeling, littoral zone mapping, and archeological and geological applications. The accuracy and resolution depend on application, and several technologies are usually available that can meet any application requirements. The ability to generate accurate IfSAR DEMs at regional to global scales quickly and at a reasonable cost has seen the rapid infusion of this technology into a variety of applications.

### ***Topographic Mapping***

Topographic maps similar or identical in nature to aerial photo derived maps are being successfully generated from IfSAR data [Tighe, 2000; Tighe and Chamberlain, 2009]. IfSAR technologies have advanced to the point where centimeter-level accuracies are possible. These high-resolution systems are making their way into aerial photography niches, especially in areas inaccessible by photogrammetric systems due to cloud cover or congested airspace.

### ***Vegetation Mapping and Land Use Classification Maps***

The use of interferometry for land use classification and vegetation parameter determination is a rapidly expanding area of research [Engdahl, M., 2013.]. The use of multi-frequency IfSAR systems that exploit the relative penetration into the canopy, and the use of interferometric correlation which is sensitive to the vertical structure of the canopy, have shown great promise for extracting canopy parameter elevations [Rodriguez, Martin and Michel, 1999]. Land use maps that have classification accuracy in the 90% level have been demonstrated using data from airborne IfSAR systems [Rodriguez, Martin and Michel, 1999] and [Tighe, 2012]. Although significant ambiguities were observed under certain conditions. Specifically, problems arose due to the sensitivity to the absolute calibration of the radar **backscatter** and from changes in backscatter as a function of incidence for the same ground cover type. Using multi-frequency, multi-temporal or other optical data sources can significantly reduce classification error.

### **Urban Mapping**

Urban mapping varies from the relatively low density and simple structures of a suburb to the extremely complex and high density environment of a modern major city. Multiple scattering, shadow and layover make urban mapping a challenging application environment for IfSAR systems. High resolution airborne IfSAR systems have shown some utility for this application particularly in medium to low density urban areas [Mercer and Gill, 1998]. System resolution and the degree of algorithm optimization for urban environments greatly affect the achievable mapping accuracy [Grey et al., 2003].

### **Geological Mapping**

Topographic maps have traditionally played a key role in geological applications. IfSAR system height and image data can simultaneously provide topographic information at two scales. Using the topographic data directly, topography at the DEM posting provides information about geologic structures such as faults, volcanic structures, and alluvial fan size and extent. The associated SAR imagery, which is sensitive to the surface roughness on the scale of the radar wavelength, provides information about the micro-topography of the surface. The combination of the two scales can be used to infer information about the surface geology such as the relative age of lava flows and lithology [Tighe et al., 2006].

### **Ice Mapping**

Change in ice sheet topography is an important metric in quantifying and understanding the impacts of climate change. Most measurement of ice sheets to monitor topographic change has used either spaceborne or airborne lidar systems. Satellite radar altimetry is most accurate over flat areas, but performs poorly over the steep coastal regions where substantial amounts of change are located. Airborne laser altimetry is better suited to these steep regions but is limited in spatial coverage and swath width (500 m), thus making it impractical for use at the continental scale over Antarctica. Airborne IfSAR systems (e.g. Glisten) have been designed to provide a wide swath ice topography measurement with high precision to augment lidar ice topography measurements [Hensley et al, 2009, 2010, 2016].

### **Littoral Zone Mapping**

Littoral zone mapping is an area where IfSAR mapping is playing an increasingly key role because it maps from the near shore regions out onto the water surface<sup>4</sup>. Photogrammetric and topographic lidar systems have greater difficulty mapping these regions because neither type of system makes height measurements over water bodies. By mapping at low tides IfSAR systems should provide some of the most complete and detailed maps of the littoral zone.

### **Hydrology**

The insurance industry as well as local and national governments have become increasingly concerned about proper risk assessment associated with flooding. Risk assessment is needed for flood warning, flood plain management and financial liability studies. Flood

---

<sup>4</sup> Mapping water body surfaces is usually only possible for higher frequency systems (C-band and above) and when there is sufficient wind or current to make the water appear rough at the imaging wavelength.

plain mapping and risk assessment uses a combination of topography and surface cover type along with propagation models to determine depth of flooding. Airborne derived IfSAR DEMs with the combination of accuracy and resolution and cost have proved ideal for regional flood risk assessment as has been shown in several studies both in the United Kingdom [Galy and Sanders, 2000] and in the United States.

### **Seismic Hazards**

**Slope** and along-slope and cross-slope **curvature** estimates are needed for slope hazard analysis. Special care must be taken in computing slope and surface curvature from interferometric DEMs because point-to-point height noise can be comparable to a significant fraction of the post spacing. Studies have shown that when this is considered, IfSAR derived DEMs improve classification of areas of landslide induced seismic risk [Real et al, 1997].

### **Environmental Disasters**

Data and products supplied by the COSMO-SkyMed system represent a valid and important instrument, to carry on studies about causes and phenomena preceding environmental disasters as well as to improve the monitoring and evaluation of damages in case, for example, of landslips, flood, earthquakes and volcanic eruptions. Observation within a specific area can be made during day or night and even in case of clouds, thus allowing evaluations of superficial alterations of the territory and providing institutions in charge of managing the risk with a new and useful instrument of prevention and control.

### **Archeology**

Understanding where, how and when ancient civilizations modified and controlled their physical environment is an aspect of archeological research where SAR and IfSAR systems have made important contributions. Multiple frequency observations that penetrate dense vegetation coupled with accurate topographic information is providing archeologists with unique regional scale observations of ancient sites such as Angkor Wat in Cambodia and the Great Wall in China. Because of the unique perspective, SAR and IfSAR systems can provide, the use of these data in future investigations is expected to increase.

## **MAPPING ALASKA – AMERICA’S LAST FRONTIER**

This section details a large area mapping project using the IfSAR technology. Here the reader will gain an insight on how this technology provided the only available DEM generating technique solution to map America’s last frontier.

### ***The Alaska DEM Whitepaper***

At the 2008 Alaska Surveying and Mapping Conference in Alaska, surveying and mapping firms in attendance were asked to provide suggestions on the best way to map Alaska. This information was invited because the state of Alaska had never been mapped at any scale meeting the National Map Accuracy Standards, thus, leaving it the only US state without statewide digital orthophotos or elevation data comparable to accuracies held by continental United States (CONUS). Immediately it became apparent the importance of collecting an accurate elevation dataset, prior to producing orthophotos (which benefit

from accurate and homogenous elevation data). Dewberry was hired, based on their knowledge of varied DEM technologies from many commercial companies and their quality assurance procedures that are highly regarded in the mapping industry, to prepare what is commonly known as the Alaska DEM Whitepaper [Dewberry, 2008].

In researching the Alaska DEM Whitepaper, Dewberry learned that the state and various federal agencies had been trying for decades to determine the best solution for mapping the state. Dewberry learned that Alaska had America's worst geodetic and geospatial infrastructure; had the largest area to be mapped (covering 10 UTM zones); had the longest distances from suitable airfields where aircraft could be based; had the tallest mountains and longest shorelines in the U.S.; had the highest incidents of Controlled Flight Into Terrain (CFIT) aircraft accidents; had the fewest roads and the most reliance on airfields (but with small aircraft not powerful enough to fly over mountains, but through mountain passes that must be mapped accurately); had the most impact from climate and sea level changes and the highest impact from post-glacial rebound that changed elevations and gravity. This whitepaper recommended statewide aerial IfSAR as the best solution for acquiring DTMs and DSMs, prior to production of digital orthoimagery and updates to the National Hydrography Dataset (NHD), transportation and other geospatial layers needed in Alaska. The use of IfSAR technology due to its ability to operate day and night, in such a remote large area (limited road access), varied terrain, and with little in-scene ground control placement, and short data collection timeframes (a couple of months in the summer due to weather) was the only mapping technology that could collect accurate elevation data in a short mapping season.

The Geographic Information Network of Alaska (GINA) provided examples of what happened when attempting to drape satellite imagery over the existing DEM from the National Elevation Dataset (NED). Some mountains were said to be horizontally displaced by over a mile in the NED, making it erroneously appear as though streams flowed over mountains and hills rather than through the valleys. In addition to extended periods of darkness in winter months, Alaska's valleys are often obscured by clouds and/or fog, but flights must continue under Instrument Flight Rules (IFR) to get patients to health clinics or otherwise conduct daily operations routinely executed under adverse weather conditions. IFR procedures rely on accurate elevation data. Imagine flying in the dark or through clouds, intending to be flying up a valley, but because of DEM errors in the cockpit display, the plane is unknowingly flying into an unseen mountainside. If it were a clear day, this would not be a problem when flying under Visual Flight Rules (VFR), but when flying through clouds or in the dark under IFR, having mountains mapped in the wrong place can be a fatal error. In addition to aviation safety, there was an obvious and immediate need to collect accurate statewide elevation data for production of statewide digital orthophotos as the accuracy of the DEM generated from the NED was insufficient for orthorectification.

In analyzing DEM user requirements, although some cities and high value corridors had needs for higher-accuracy, higher-cost lidar data, aerial IfSAR was Dewberry's recommendation for statewide mapping because it was the only technology that could map through clouds, because it could produce DEMs with  $RMSE_z \leq 2$  meters and  $RMSE_r \leq 8$  meters, and because it was the most affordable. Clouds had long been Alaska's nemesis for statewide mapping, but with IfSAR this was a non-issue.

### ***The Alaska Statewide Digital Mapping Initiative (SDMI)***

Officials of the Alaska Statewide Digital Mapping Initiative (SDMI) then asked USGS to use its Geospatial Products and Services Contract to contract with Dewberry to develop an overall plan for statewide IfSAR mapping, to manage IfSAR contractors and to quality control their data. With Dewberry, as prime contractor, Dewberry, Fugro EarthData and Intermap Technologies developed a joint plan in which Intermap would map the easiest (least rugged and least forested) 75% of the state with X-band IfSAR and Fugro would map the hardest 25% of the state with X-band and P-band IfSAR. Because terrain slope impacts the accuracy of IfSAR data (see Figure 7.12 above), both IfSAR firms felt they could satisfy the 2m RMSEz requirement only for slopes up to 20 degrees, assuming larger vertical errors in steeper terrain.

The IfSAR mapping started in 2010 and will continue until approximately 2019, depending on available funding. As of the end of 2016, IfSAR data has been acquired for approximately 75% of the state, with the southwestern part of the state, including the Aleutian Islands, remaining to be mapped during the next 2-3 years. The principal IfSAR deliverables include a hydro-enforced DTM with 5-meter posts, a DSM with 5-meter posts, ortho-rectified radar imagery (ORI) with 5-meter pixels or better (being delivered down to 62.5-cm pixels), in multiple file formats and projections required by the state, USGS and NGA. FGDC-compliant metadata files, a certified ISO 9001 data-quality report for each 15-minute tile, void masks and slope masks are also provided. Blind QA/QC checkpoints have been surveyed statewide by JOA Surveys.

Figure 7.31 shows an example hydro-enforced DEM from Intermap and Figure 7.32 shows the comparable DEM previously available from the NED. Both images are courtesy of Intermap. Because hydrologic modeling, and updating the obsolete NHD datasets, are among the most critical user requirements in Alaska, the new IfSAR data are vital for management of Alaska's vast natural resources, including water. Water boundaries are "loud and clear" with IfSAR data whereas they are often questionable with optical imagery or lidar.

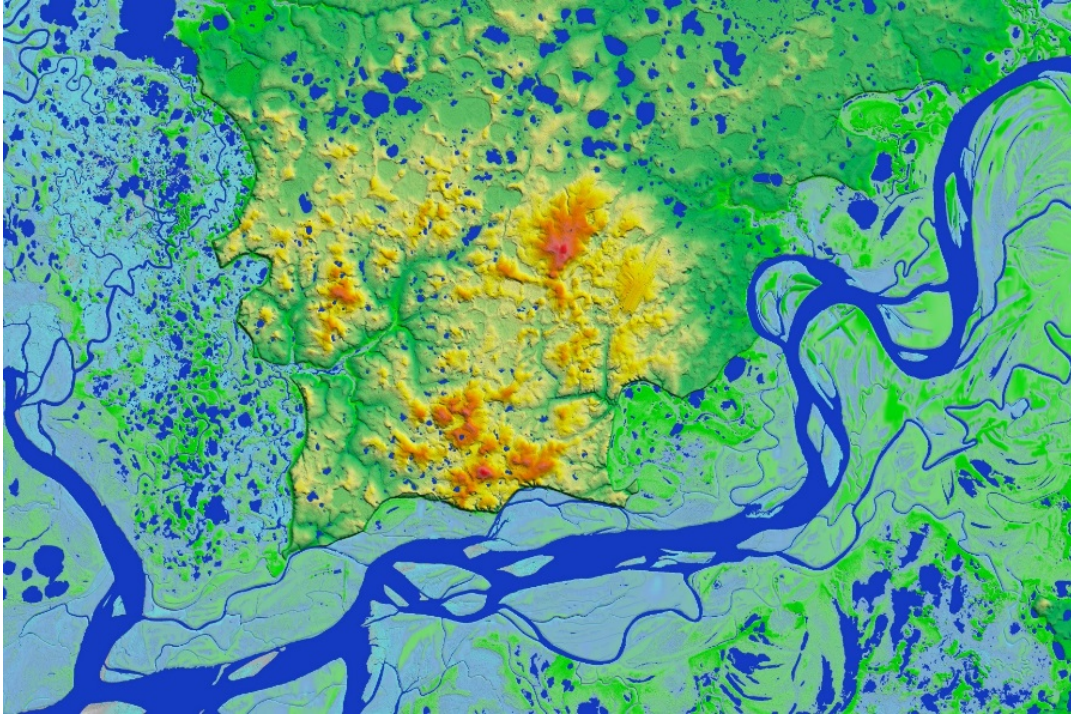


**Figure 7.31. IfSAR data showing complex hydrographic features very important in Alaska where water resources are of critical importance.**

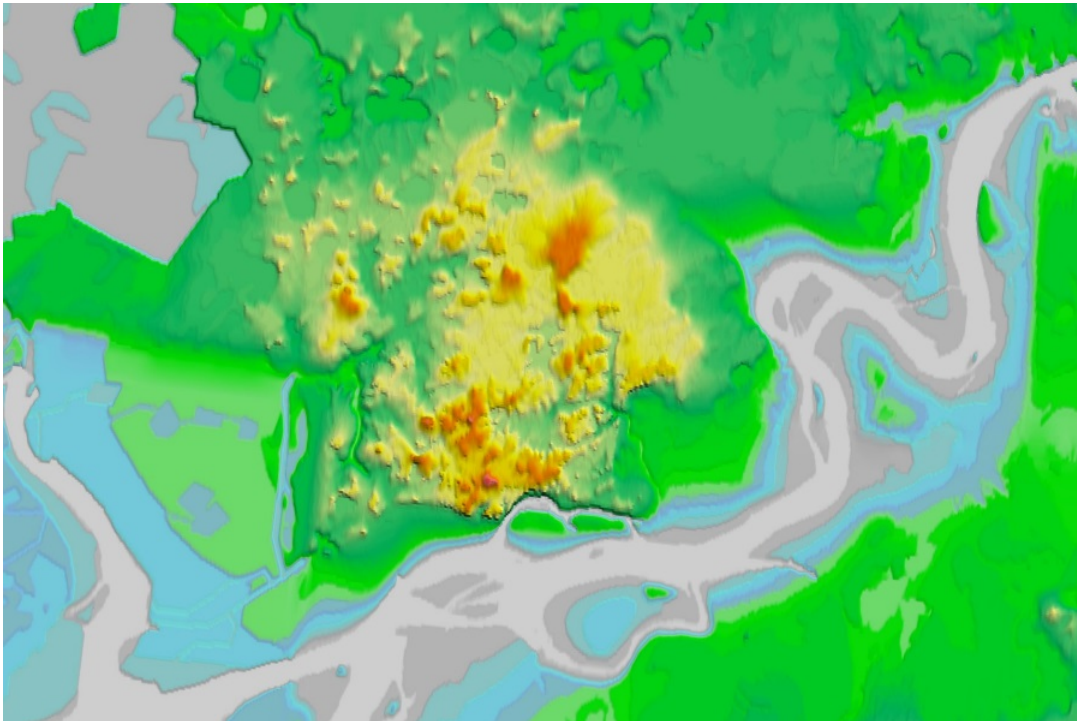


**Figure 7.32. NED data covering the same geographic extent as the IfSAR in Figure 7.31 but with minimal hydrographic features shown.**

## DIFFERENTIAL INSAR METHOD

The section provides an example of using IfSAR technology in an advanced configuration called differential InSAR or DInSAR for short. Radar targets can be Permanent Scatter (PS) (e.g., buildings, rock outcrops) or Distributed Scatter (DS) (e.g., fallow fields, roadways). The processing of a long series of radar images using the DInSAR technique allows the motion history of a radar target to be observed (including non-linear motion), and increases measurement precision to millimeter level (Ferretti, et al, 2000; Ferretti, et al., 2011). DInSAR technique is typically used to monitor subsidence/uplift or lateral deformation.

The DInSAR technique involves using multi-interferometric outputs created from using many radar images (at least 15-20) acquired over the same area with the same acquisition mode and geometry. The resulting DInSAR interferogram series is then, a comprehensive history of changes in ground movement or displacement (Ferretti, et al., 2000).

Surface movement is determined by the spatial variation of phase across the image over several pixels. When using the DInSAR technique to identify surface movements of millimeter to centimeter scale with high spatial resolution it is necessary to remove topographic and atmospheric effects. To ensure that the interferogram measurements have topography removed from the DInSAR data, the topographic phase is often simulated using a reference DEM (or if possible an IFSAR derived DEM is used) and then removed from the interferogram.

Atmospheric artefacts show a strong spatial correlation within every single SAR acquisition, but are uncorrelated in time. Conversely, target motion is usually strongly correlated in time and can exhibit different degrees of spatial correlation depending on the phenomenon at hand. When long time-series of SAR images are combined, atmospheric effects can be estimated, modelled and removed based on these different correlation patterns. To exploit all the available images, and improve the accuracy of estimation, only coherent scatters (targets) are selected.

### **DInSAR Example - Coastal Subsidence Monitoring over Hampton Roads**

Coastal risk management is a complex equation that must take into consideration changing land and maritime conditions. Within this equation, subsidence can strongly impact sensitive and at-risk areas, particularly when coupled with sea level rise.

Hampton Roads is located within the southeastern corner of the state of Virginia, USA. This coastal inlet is predominantly urban and has the largest concentration of federal bodies and facilities of any metropolitan area in the world. This area is experiencing some of the highest rates of sea level rise, in part due to land subsidence related to compaction of aquifers within.

A DInSAR analysis was carried out over Hampton Roads to assess to quantify subsidence rates. This was accomplished using 130 Cosmo-SkyMed SAR images covering a six-year period between 13 July 2011 and 28 August 2017. A considerable number of localized movement features and wider-area trends were detected, such as the localized subsidence observed over the East Ocean View neighborhood as shown in Figure 7.33.

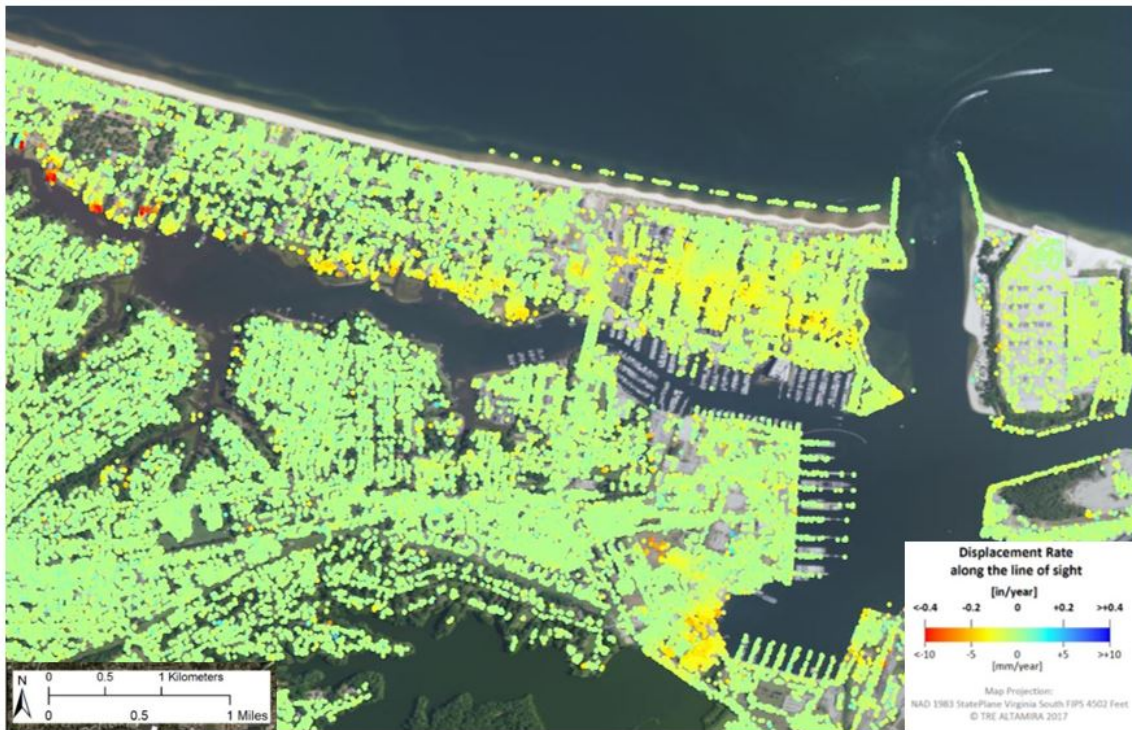


Figure 7.33. A total of 4,150,248 measurement points was identified over the processed area, exhibiting an average displacement rate of -0.04 inches/year (-1.0 mm/year) with an associated confidence limit of  $\pm 0.01$  inches/year ( $\pm 0.35$  mm/year).

Examples of time series are shown in Figures 7.34 and 7.35.

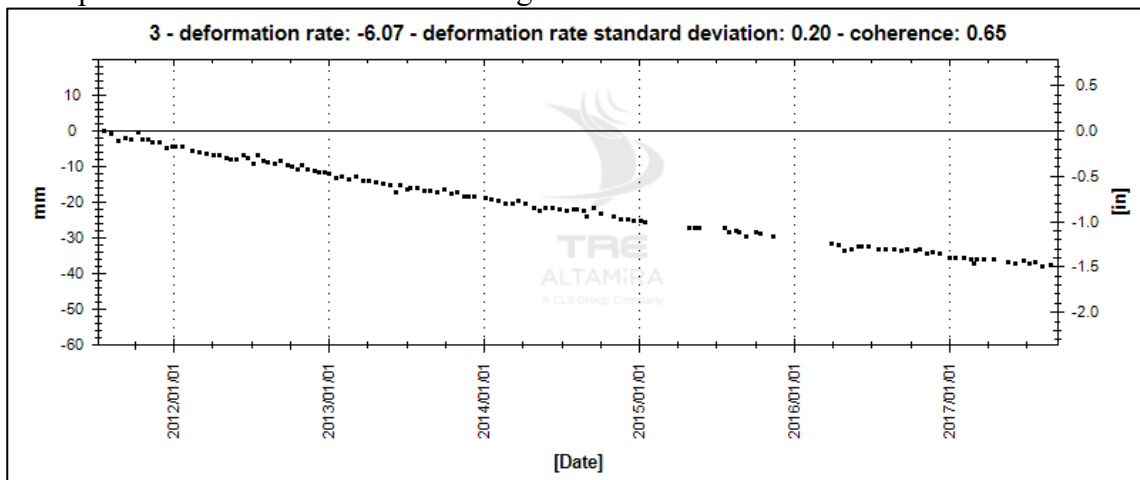


Figure 7.34. Example of time series identified over Tanner Point, within the Virginia Port area.

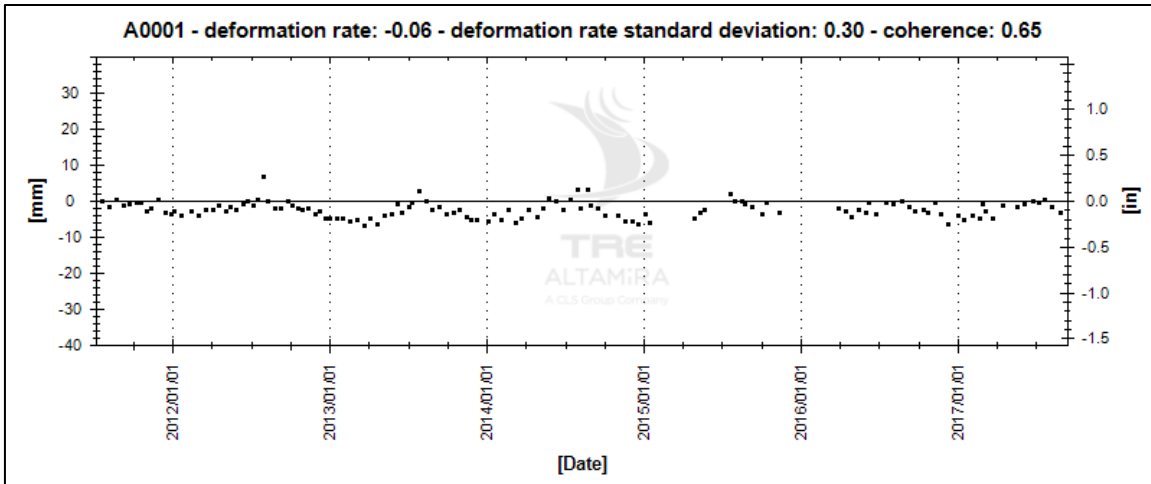


Figure 7.35. Seasonal variation captured from measurement points identified over part of the W Norfolk Bridge.

A cross section over the George Washington overpass was selected to illustrate the DInSAR technique used to observe subsidence (Figure 7.36). DInSAR results viewed as surface profile cross-sections (Figure 7.36) illustrate subsidence dynamics over time where each individual profile corresponds to ground displacement compared to the first acquired SAR image. While the George Washington overpass is stable, both ramps are showing over -4.5 inches (-115.0 mm) of subsidence over the period of this analysis (Figure 7.37).



Figure 7.36. A cross-section over the George Washington overpass illustrating differential subsidence patterns in this area.

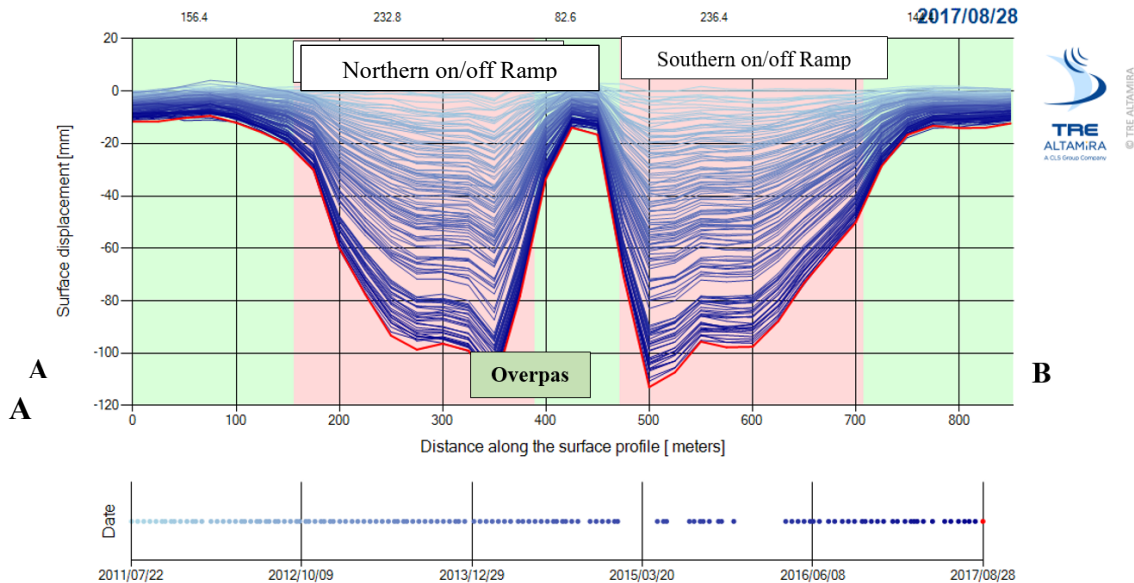


Figure 7.37: Surface profile cross-section corresponding to the trace illustrated in Figure 7.35.

## TECHNOLOGICAL ADVANCEMENTS

The success of the IfSAR/InSAR technology over the past two decades has provided a plethora of DEM generation platforms. Continued advances in IfSAR/InSAR technology have led the way for the deployment of SAR satellite constellations such as Europe's Copernicus program (10 Satellites: 5 tandem pairs, 2 orbital planes) and Urthecast OptiSAR™ Constellation (16 Satellites: 8 tandem pairs, 2 orbital planes) which will continuously observe the earth every day, every night, rain or shine, revolutionizing the world's ability to monitor our planet regardless of obstacles like tree cover and weather phenomena. Such constellations provide high reliability, improved revisit time, geographical coverage, and rapid SAR and IfSAR/InSAR data collection and dissemination to support operational applications in the priority areas of marine monitoring, land monitoring, and emergency services. To promote wider use of IfSAR data products, to increase research on interferometric techniques and to make it easier for people to produce accurate IfSAR measurements, IfSAR providers will develop web-based tools which, through a user-friendly interface, which enable users to generate IfSAR products from the spaceborne data repositories, in a matter of minutes.

What's Next with SRTM? Engineers and scientists at JPL are currently working on a complete reprocessing of the original SRTM radar data to produce an improved near-global digital elevation model (DEM) to be called NASADEM. As with SRTM Plus, this work is funded under NASA's "Making Earth System Data Records for Use in Research Environments" (MEaSUREs) Program. In brief, the expected improvements include (1) fine vertical adjustments within and among individual shuttle data takes via reference to precise ICESat (Ice, Cloud, and land Elevation Satellite) laser profiles, (2) void reduction via improved radar interferometric processing, (3) use of better fill data in the remaining voids, especially ASTER GDEM3 when available, and (4) improved quality assessments and adjustments. This project is scheduled for completion in 2017.

With the success of the Tandem-X mission, DLR has demonstrated its pioneering role and satisfied the prerequisites for the next major development step in satellite-based

Earth observation – the Tandem-L radar mission. The Tandem-L successor mission could provide a current elevation image of Earth’s entire landmass every eight days and thereby capture dynamic processes in a timely manner. This would also make it possible to contribute to the review of international climate and environmental agreements. New radar methods and innovative missions such as Tandem-L are set to contribute to gaining a better understanding of dynamic processes to protect and preserve Earth. Completion of the TanDEM-X global elevation model has now paved the way for the next dimension of radar remote sensing.

## ACKNOWLEDGEMENTS

The principal authors for this chapter are Dr. Scott Hensley, Radar Science and Engineering Section, Jet Propulsion Laboratory and Dr. Lorraine Tighe Strategic Geospatial Services, LLC. Contributing authors include Dr. David Maune of Dewberry who contributed the Mapping Alaska section; Jessica Morgan of TRE Altamire Inc. who contributed the section on the Differential InSAR (DInSAR) method; and Dr. Riadh Munjy and Dr. Paul Rosen who co-authored some of the materials re-used from the 1<sup>st</sup> and 2<sup>nd</sup> editions of this manual.

Scott Hensley (SM’10-F’14) received his BS degrees in Mathematics and Physics from the University of California at Irvine and the Ph.D. in Mathematics from Stony Brook University where he specialized in the study of differential geometry. In 1992, Dr. Hensley joined the staff of the Jet Propulsion Laboratory where he is currently a Senior Research Scientist studying advanced radar techniques for geophysical applications. He has worked on most of the SAR systems developed at JPL over the past two decades including the Magellan and Cassini radars. He was the GeoSAR Chief Scientist, a simultaneous X-band and P-band airborne radar interferometer for mapping above and beneath the canopy that is now commercially operated by Earthdata International. He led the SRTM Interferometric Processor Development Team for a shuttle based interferometric radar used to map the Earth’s topography between  $\pm 60^\circ$  latitude. He also employed the Earth-based Goldstone Solar System Radar to generate topographic maps of the lunar surface. He was Principal Investigator and is currently the Project Scientist for the NASA UAVSAR program which is an electronically scanned active array L-band fully polarimetric radar designed for repeat pass applications.

Lorraine Tighe has a Ph.D. degree in Earth Sciences, a graduate diploma in Remote Sensing, and a B.Sc. degree in Physics and Geology. Lorraine is currently the Senior Remote Sensing Product Marketing lead at Esri. She has been involved with IfSAR research for topographic and geological mapping and forestry applications for the past 23 years. Dr. Tighe’s research activities include studying the amount of X-band penetration into open barren terrain and vegetated canopy using Intermap data as well as simultaneous L and C band TOPSAR measurements and repeat pass airborne interferometry data utilized to generate worldwide elevation models from IfSAR techniques. She has delivered lectures, workshops and training sessions in Canada, United States of America, Jamaica, Brazil, Equator, Honduras, England, Scotland, Poland, Germany, Indonesia, Philippines, Malaysia, and Australia.

## REFERENCES

Andersen, H.-E., Reutebuch, S.E., and McGaughey, R.J. (2005). Accuracy of an IfSAR derived digital terrain model under a conifer forest canopy. In *Canadian Journal of*

- Remote Sensing*, 3, 1, (pp.1-6). URL: <http://www.tandfonline.com/doi/abs/10.5589/m05-016?journalCode=ujs20>.
- Andersen, H. -E., R. J. McGaughey, and S. E. Reutebuch (2008). Assessing the influence of flight parameters, interferometric processing, slope and canopy density on the accuracy of X-band IfSAR-derived forest canopy height models. In *International Journal of Remote Sensing*, 29(5), (pp.1495-1510). URL: <https://www.treearch.fs.fed.us/pubs/29944>.
- ASPRS (2014). ASPRS positional accuracy standards for digital geospatial data. In *Photogrammetric Engineering and Remote Sensing*, 81(3) (pp. A1-A26), Bethesda, MD: American Society for Photogrammetry and Remote Sensing. URL: <https://www.asprs.org/pad-division/asprs-positional-accuracy-standards-for-digital-geospatial-data.html>.
- Bamler, R. and Hartl, P. (1998). Synthetic aperture radar interferometry. In *Inverse Problems*, Vol.14, No. 4: R1-54. URL: <http://iopscience.iop.org/article/10.1088/0266-5611/14/4/001/pdf>.
- Boerner, W-M, H. Mott, E. Lüneburg, C. Livingston, B. Brisco, R. J. Brown and J. S. Paterson with contributions by S.R. Cloude, E. Krogager, J. S. Lee, D. L. Schuler, J. J. van Zyl, D. Randall P. Budkewitsch and E. Pottier (1998). Polarimetry in radar remote sensing: basic and applied concepts, Chapter 5 in F.M. Henderson, and A.J. Lewis, (eds.), Principles and Applications of Imaging Radar, Vol. 2 of *Manual of Remote Sensing*, 3rd Ed., New York, NY., John Willey & Sons. URL: <https://hal.archives-ouvertes.fr/hal-00787303>.
- Cloude, S. R., and K. P. Papathanassiou (1998). Polarimetric SAR interferometry. In *IEEE Transactions on Geoscience and Remote Sensing*, 36(5), (pp.1551-1565). URL: <http://ieeexplore.ieee.org/document/718859/>.
- Dewberry (2008). Digital elevation model (DEM) data for the Alaska Statewide Digital Mapping Initiative (SDMI), September 18, 2008. URL: [http://agc.dnr.alaska.gov/documents/Alaska\\_SDMI\\_DEM\\_Whitepaper\\_Final.pdf](http://agc.dnr.alaska.gov/documents/Alaska_SDMI_DEM_Whitepaper_Final.pdf).
- Elachi, C. (1988). Spaceborne Radar Remote Sensing: Applications and Techniques. New York: IEEE Press, 288p.
- Engdahl, M.(2013). Multitemporal insar in land-cover and vegetation mapping. URL: <http://lib.tkk.fi/Diss/2013/isbn9789526054162/isbn9789526054162.pdf>.
- Farr, T. G., Paul A. Rosen, Edward Caro, Robert Crippen, Riley Duren, Scott Hensley Michael Kobrick, Mimi Paller, Ernesto Rodriguez, Ladislav Roth, David Seal, Scott Shaffer, Joanne Shimada, Jeffrey Umland, Marian Werner, Michael Oskin, Douglas Burbank, and Douglas Alsdorf (2007). The shuttle radar topography mission. In *Reviews of Geophysics.*, 45, RG2004, doi:10.1029/2005RG000183. URL: <http://onlinelibrary.wiley.com/doi/10.1029/2005RG000183/supinfo>.
- Ferretti, A., Fumagalli, A., Novali, F., Prati, C., Rocca, F., and Rucci, A. (2011). A new algorithm for processing interferometric data-stacks: SqueeSAR. In *IEEE Transactions on Geoscience and Remote Sensing*, (pp. 3460-3470). URL: <http://ieeexplore.ieee.org/document/5765671/>
- Ferretti, A., Prati, C., & Rocca, F. (2000). Non- linear subsidence rate estimation using the permanent scatters in differential SAR interferometry. In *IEEE Transactions on Geoscience and Remote Sensing*, (pp. 8-20). URL:

- [https://www.researchgate.net/publication/3202453\\_Nonlinear\\_subsidence\\_rate\\_estimation\\_using\\_permanent\\_scatterers\\_in\\_differential\\_SAR\\_Interferometry](https://www.researchgate.net/publication/3202453_Nonlinear_subsidence_rate_estimation_using_permanent_scatterers_in_differential_SAR_Interferometry)
- Garestier, F., Dubois-Fernandez, P., Papathanassiou, K. (2008). Pine forest height inversion using single-pass X-band PolInSAR data. URL: <http://ieeexplore.ieee.org/document/4384457/>.
- Gens, R. (2002). Introduction to SAR interferometry. Presentation given at the University of Fairbanks. URL: [http://www.asf.alaska.edu/~rgens/teaching/asf\\_seminar/intro\\_insar.pdf](http://www.asf.alaska.edu/~rgens/teaching/asf_seminar/intro_insar.pdf).
- Graham, L. C. (1974). Synthetic interferometric radar for topographic mapping. In *Proc. IEEE*, 62(6), (pp. 763-768). URL: <http://ieeexplore.ieee.org/document/1451446/>.
- Grey, W.M.F., Luckman, A. J., D Holland (2003). Mapping urban change in the UK using satellite radar interferometry. In *Remote Sensing of Environment*, Volume 87, Issue 1, 15 September, (pp. 16–22). URL: <http://www.sciencedirect.com/science/article/pii/S0034425703001421>.
- Hajnsek, I., Kugler, F., Lee, S. K., and Papathanassiou, K. P. (2008). Tropical forest parameter estimation by mean of Pol-InSAR: the INDREX-II campaign. In *IEEE Transactions on Geoscience and Remote Sensing*, Vol. 47, No. 2 (pp. 481-493). URL: <https://pdfs.semanticscholar.org/3828/961fca0022d8e8cb0f0c6d2187dfd9814bed.pdf>.
- Hensley, S. and Webb, F. H. (1994). Comparison of long valley TOPSAR data with kinematic GPS measurements. In *IGARSS Proceedings*, Pasadena, CA. URL: <https://ntrs.nasa.gov/search.jsp?R=20060039744>.
- Hensley, S., Chapin, E., Freedman, A., Le, C., Madsen, S., Michel, T., Rodriguez, E., Siqueira, P. and Wheeler, K. (2001). First P-band results using the GeoSAR mapping system. In *Proceedings of IGARSS 2001*, Sydney, Australia. URL: <http://ieeexplore.ieee.org/document/976078/>.
- Hensley, Scott, Eric Gurrola, Leif Harcke, Martin Slade, Kevin Quirk, Meera Srinivasan, Clement Lee, Sang-Ho Yun, Joseph Jao, Barbara Wilson, Eric De Jong, and Nick Marechal (2010). Lunar topographic mapping using a new high-resolution mode for the GSSR radar. In *Radar Conference, 2010 IEEE*. URL: <http://ieeexplore.ieee.org/document/5494575/>.
- Hensley, Scott, Eric Gurrola, Paul Rosen, Martin Slade, Joseph Jao, Mike Kobrick, Barbara Wilson, Curtis Chen and Raymond Jurgens (2009). An improved map of the lunar south pole with earth based radar interferometry. Radar conference, 2008). URL: <http://ieeexplore.ieee.org/document/4721077/>.
- Hensley, Scott, Thierry Michel, Maxim Neumann, Marco Lavallo, Razi Ahmed, Ron Muellerschoen and Bruce Chapman (2014). A comparison of multi-baseline polarimetric interferometry at La Amistad and La Selva, Costa Rica with a modified PolSARProSim scattering tool. In *Proceedings of EUSAR 2014*. URL: <http://ieeexplore.ieee.org/document/6856722/>.
- Hensley, S., K. Wheeler, G. Sadowy, C. Jones, S. Shaffer, H. Zebker, T. Miller, B. Heavey, E. Chuang, R. Chao, K. Vines, K. Nishimoto, J. Prater, B. Carrico, N. Chamberlain, J. Shimada, M. Simard, B. Chapman, R. Muellerschoen, C. Le, T. Michel, G. Hamilton, D. Robison, G. Neumann, R. Meyer, P. Smith, J. Granger, P. Rosen, D. Flower, R. Smith (2008). The UAVSAR instrument: description and first results. In *IEEE Radar Conference*, 6 pp. URL: <http://ieeexplore.ieee.org/document/4720722/>.

- Hensley S, Moller D, Oveisgharan S, Michel T & Wu X (2016). Ka-band mapping and measurements of interferometric penetration of the Greenland ice sheets by the GLISTIN radar. In *IEEE Journal of Selected Topics in Applied Earth Observations and Remote Sensing*, 9(6), DOI: 10.1109/JSTARS2560626. URL: <http://ieeexplore.ieee.org/document/7480354/>.
- Intermap (2011). Intermap product handbook. URL: <http://info.intermap.com/product-handbook.html?site=product-handbook>.
- Kobayashi, Y., K. Sarabandi, L. Pierce, and M. C. Dobson (2000). An evaluation of the JPL TOPSAR for extracting tree heights. In *IEEE Transactions on Geoscience and Remote Sensing*, 38, (pp. 2446-2453). URL: <https://web.eecs.umich.edu/~saraband/KSIEEE/J49IEEETGRSNov00Kobayashi.pdf>.
- Lewis, A. J. and Henderson, F. M. (1999). Radar fundamentals: the geoscience perspective. In *Principles and Application of Imaging Radar: Manual of Remote Sensing*, 3<sup>rd</sup> edition, Robert A. Ryerson (Ed.), New York, NY, Wiley. URL: <https://searchworks.stanford.edu/view/3883741>.
- Li, F. and Goldstein, R.M. (1990). Studies of multibaseline spaceborne interferometric synthetic aperture radar. In *IEEE Trans. Geosci. Remote Sensing*, 28(1), (pp. 88-97). URL: <http://ieeexplore.ieee.org/document/45749/>.
- Madsen, S. N., Zebker, H. A. and Martin, J. (1993). Topographic mapping using radar interferometry: processing techniques. In *IEEE Trans. Geosci. and Rem. Sens.*, 31(1), (pp. 246-256). URL: <http://ieeexplore.ieee.org/document/210464/>.
- Mercer, J. B. and Gill, M. (1998). Radar-derived DEMs for urban areas. In *Proceedings of the ISPRS Commission IV Symposium*, Stuttgart, Germany. URL: <http://www.isprs.org/proceedings/XXXII/part4/merc7.pdf>.
- Moller, D., Hensley, S., Sadowy, G.A., Fisher, C.D., Michel, T., Zawadzki, M., Rignot, E. (2011). The Glacier and Land Ice Surface Topography Interferometer: An Airborne Proof-of-Concept Demonstration of High-Precision Ka-Band Single-Pass Elevation Mapping. In *IEEE Transactions on Geoscience and Remote Sensing*, IEEE Transactions on, vol.49, no.2, (pp.827-842), Feb. 2011, doi: 10.1109/TGRS.2010.2057254. URL: <http://ieeexplore.ieee.org/document/5560792/>.
- Positional Accuracy Handbook* (1999). Minnesota Planning Land Management Information Center. URL: [https://www.metrogis.org/MetroGIS/media/gis-documents/how-do-i-get/MnGeoStandardsCommittee\\_PositionalAccuracyHandbook.pdf](https://www.metrogis.org/MetroGIS/media/gis-documents/how-do-i-get/MnGeoStandardsCommittee_PositionalAccuracyHandbook.pdf)
- Schneider, R. Z., K. P. Papathanassiou, I. Hajnsek, and A. Moreira (2006). Polarimetric and interferometric characterization of coherence scatters in urban areas. In *IEEE Transactions on Geoscience and Remote Sensing*, 44(4), (pp. 971-984). URL: [https://www.researchgate.net/profile/Alberto\\_Moreira/publication/220052717\\_Polarimetric\\_and\\_Interferometric\\_Characterization\\_of\\_Coherent\\_Scatterers\\_in\\_Urban\\_Areas/links/004635200a04545718000000/Polarimetric-and-Interferometric-Characterization-of-Coherent-Scatterers-in-Urban-Areas.pdf](https://www.researchgate.net/profile/Alberto_Moreira/publication/220052717_Polarimetric_and_Interferometric_Characterization_of_Coherent_Scatterers_in_Urban_Areas/links/004635200a04545718000000/Polarimetric-and-Interferometric-Characterization-of-Coherent-Scatterers-in-Urban-Areas.pdf).
- Raney, K. (1999). Radar fundamentals: technical perspective. In *Manual of Remote Sensing*, 3<sup>rd</sup> edition, Ch 2, Boston, MA: Artech House. URL:
- Real, C., Wilson, R. I. and McCrink, T. P. (1997). Suitability of airborne-radar topographic data for evaluating earthquake-induced ground failure hazards. In *12th Int. Conf. on Appl. Geol. Rem. Sens.*, Denver, CO. URL:

- <https://www.tib.eu/de/suchen/id/BLCP%3ACN022901692/Suitability-of-Airborne-Radar-Topographic-Data/>.
- Rabus, B, M. Eineder, A. Roth, and R. Bamler (2003). The shuttle radar topography mission—a new class of digital elevation models acquired by spaceborne radar. In *ISPRS Journal Photogrammetry and Remote Sensing*, 57(4), (pp. 241–262). URL: <http://www.sciencedirect.com/science/article/pii/S0924271602001247>
- Richards, M. A. (2007). A beginner’s guide to interferometric SAR concepts and signal processing. In *IEEE Aerospace and Electronic Systems Magazine*, 22(9), (pp. 5-29). URL: <http://ieeexplore.ieee.org/document/4350281/>.
- Slater, J. A., G. Garvey, C. Johnston, J. Haase, B. Heady, G. Kroenung, and J. Little (2006). The SRTM data “finishing” process and products. In *Photogrammetric Engineering and Remote Sensing*, 72(3), (pp. 237-247). URL: <http://citeseerx.ist.psu.edu/viewdoc/download?doi=10.1.1.404.2304&rep=rep1&type=pdf>.
- Smith, B., and D. Sandwell (2003). Accuracy and resolution of shuttle radar topography mission data. In *Geophysical Research Letters*, 30, (pp. 1467-1470). URL: <http://topex.ucsd.edu/sandwell/publications/97.pdf>.
- Tighe, M. L. (2012). Empirical assessment of multi-wavelength, synthetic aperture radar for land cover and canopy height estimation. Ph.D. Thesis, Carleton University, 251p. URL: <http://adsabs.harvard.edu/abs/2012PhDT.....215T>
- Tighe, M.L., D. King, H. Balzter, A. Bannari, and H. McNairn (2012). Airborne X-HH incidence angle impact on canopy height retrieval: implications for spaceborne X-HH Tandem-X global canopy height models. In *XII Congress of the International Society for Photogrammetry and Remote Sensing*, Melbourne, Australia, <http://www.isprs2012.org/abstract/1595.asp>.
- Tighe, M. L. and D. Chamberlain (2009). Accuracy comparison of the SRTM, ASTER, NED and NEXTMap USA digital terrain model over several USA study sites. ASPRS/MAPPS Fall Conference, San Antonio, Texas, 12p. URL: <https://www.semanticscholar.org/paper/Accuracy-Comparison-of-the-Srtm-Aster-Ned-Nextmap-Tighe/55aacab455a8f25b663c5cbfe98afc294f9b1fc1>.
- Tighe, M. L., T. Said, and I. Ipranta (2006). Three-dimensional visualization of orthorectified radar imagery and digital elevation models used to generate a 1:50,000-scale geology map for Amurang, Sulawesi, Indonesia. In *Map Asia Conference*, 9p.
- Tighe M. L. (2000). Topographic line maps production using high resolution airborne interferometric SAR. In *International Archives of Photogrammetry and Remote Sensing*. Vol. XXXIII, Part B4. Amsterdam, 2000, (pp. 602-608). [http://www.isprs.org/proceedings/XXXIII/congress/part4/602\\_XXXIII-part4.pdf](http://www.isprs.org/proceedings/XXXIII/congress/part4/602_XXXIII-part4.pdf)
- Zebker, H. A. and Goldstein, R. M. (1986). Topographic mapping from interferometric SAR observations. In *J. Geophys. Res.*, 91, (pp. 4993-4999). URL: <http://onlinelibrary.wiley.com/doi/10.1029/JB091iB05p04993/abstract>.
- Zebker, H. A., Rosen, P. A. and Hensley, S. (1997). Atmospheric effects in interferometric synthetic aperture radar surface deformation and topographic maps. In *J. Geophys. Res.*, 102, (pp. 7547-7563). URL: <http://onlinelibrary.wiley.com/doi/10.1029/96JB03804/abstract>
- Zebker, H.A. and Villasenor, J. (1992). Decorrelation in interferometric radar echoes. In *IEEE Trans. Geosci. Rem. Sens.*, vol. 30, (pp. 950-959). URL:

[https://www.researchgate.net/publication/3201038\\_Decorrelation\\_in\\_Interferometric\\_Radar\\_Echoes](https://www.researchgate.net/publication/3201038_Decorrelation_in_Interferometric_Radar_Echoes).

